iScience

CellPress
OPEN ACCESS

Article

Non-steady diffusion and adsorption of organic micropollutants in ion-exchange membranes: effect of the membrane thickness

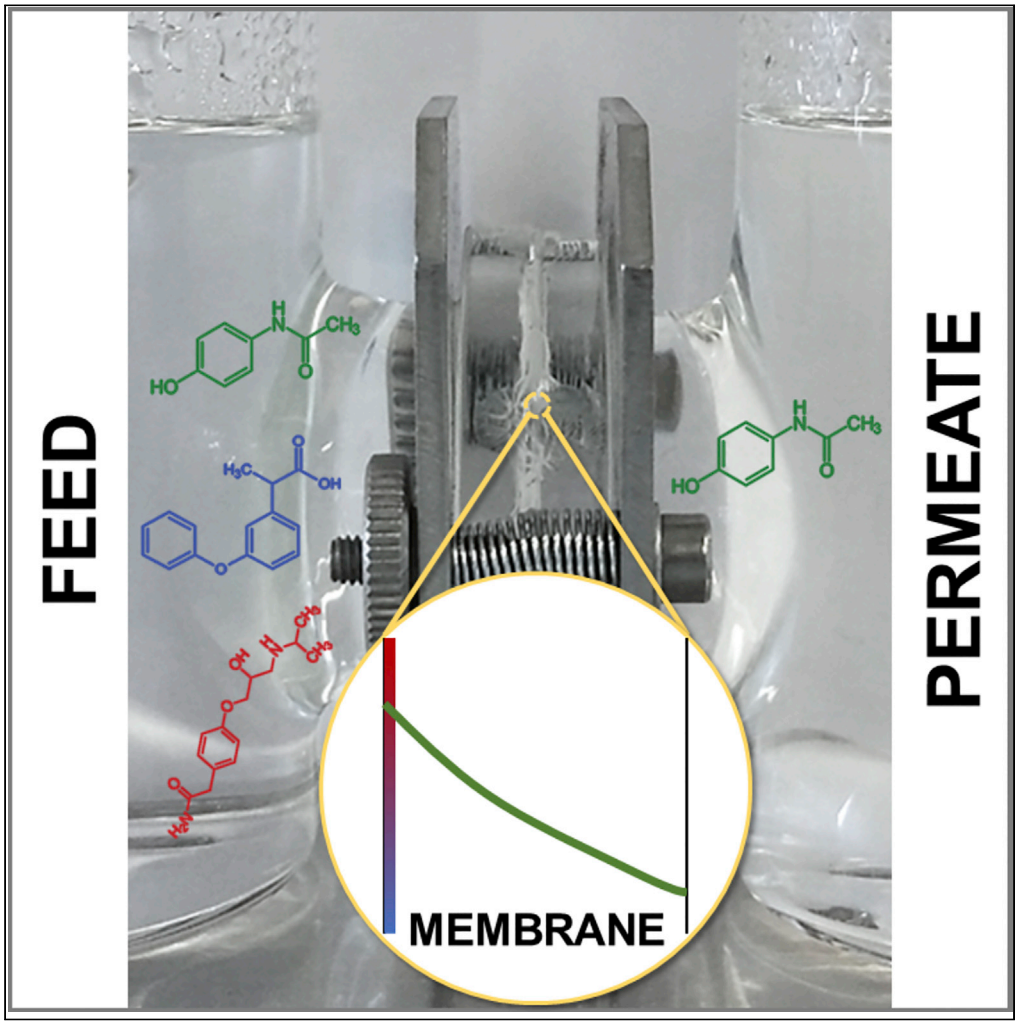

Malgorzata Roman, Pawel Roman, Rhea Verbeke, ..., Emile Cornelissen, Karel Keesman, Arne Verliefde

malgorzata.roman@wetsus.nl

HIGHLIGHTS

Electroneutrality overcomes diffusive potential of charged OMPs

The interactions between OMPs and the IEMs determine OMP transport

Adsorption influences diffusion lag time of neutral OMPs

Diffusion coefficients of neutral OMPs increased with IEMs thickness

Roman et al., iScience 24, 102095
February 19, 2021
https://doi.org/10.1016/j.isci.2021.102095

iScience

CellPress
OPEN ACCESS

Article

Non-steady diffusion and adsorption of organic micropollutants in ion-exchange membranes: effect of the membrane thickness

Malgorzata Roman,[1,2,9,*] Pawel Roman,[1] Rhea Verbeke,[3] Leonardo Gutierrez,[2,8] Marjolein Vanoppen,[2] Marcel Dickmann,[4] Werner Egger,[5] Ivo Vankelecom,[5] Jan Post,[1] Emile Cornelissen,[2,6] Karel Keesman,[1,7] and Arne Verliefde[2]

SUMMARY

There is no efficient wastewater treatment solution for removing organic micropollutants (OMPs), which, therefore, are continuously introduced to the Earth's surface waters. This creates a severe risk to aquatic ecosystems and human health. In emerging water treatment processes based on ion-exchange membranes (IEM), transport of OMPs through membranes remains unknown. We performed a comprehensive investigation of the OMP transport through a single IEM under non-steady-state conditions. For the first time, positron annihilation lifetime spectroscopy was used to study differences in the free volume element radius between anion- and cation-exchange membranes, and between their thicknesses. The dynamic diffusion-adsorption model was used to calculate the adsorption and diffusion coefficients of OMPs. Remarkably, diffusion coefficients increased with the membrane thickness, where its surface resistance was more evident in thinner membranes. Presented results will contribute to the improved design of next-generation IEMs with higher selectivity toward multiple types of organic compounds.

INTRODUCTION

The presence of organic micropollutants (OMPs) in diverse ecosystems is a direct consequence of the growing consumption of a vast amount of chemicals. OMPs comprise a broad spectrum of daily-used chemicals, e.g., pharmaceuticals, pesticides, personal care products, and plasticizers. Because of the enormous variety of their physicochemical properties, an efficient wastewater treatment solution for OMPs has not yet been developed, where the diversity of OMPs detected in waste water treatment plants effluents was widely reported (Deblonde et al., 2011; Sui et al., 2015). As a consequence of discarding treated wastewater to the environment, sewer exfiltration, and urban stormwater recharge, OMPs are continuously being introduced to aquatic environments (Bolong et al., 2009; Sirés and Brillas, 2012; Gabarrón et al., 2016; Jones et al., 2003; Osenbrück et al., 2007), where they have been detected at ng L^{-1} up to µg L^{-1} concentration range (Jobling et al., 1998; Verliefde, 2008; Tang et al., 2013; Sui et al., 2015). The global occurrence of OMPs in different water resources has raised a serious concern about their harmful effects on aquatic ecosystems and human health, and numerous investigations have reported their environmental hazard (Schwarzenbach et al., 2006; Richardson and Ternes, 2014; Murray et al., 2010; McKinlay et al., 2008; Daughton and Ternes, 1999; Ohe et al., 2004).

Increasing population, environmental changes, and uneven distribution of freshwater have affected the balance between water demand and availability worldwide. Based on the United Nations and the World Health Organization reports, 0.7–1.2 billion people suffer from water scarcity, and another 500 million will experience this in the near future. It has been predicted that in 2030 around 50% of the world population will be affected by water stress (Water, 2009). The global water scarcity issue has created enormous pressure to search for alternative drinking water resources, such as treated wastewater. Current water management strategies in many regions (e.g., Singapore, California, and Australia) have highlighted the importance of wastewater reuse (Grant et al., 2012; Vanoppen et al., 2016; Bixio et al., 2006; Tang et al., 2018). Unfortunately, the direct production of drinking water from wastewater is currently beyond reach due to

[1]Wetsus, European Centre of Excellence for Sustainable Water Technology, Oostergoweg 9, 8911 MA Leeuwarden, the Netherlands

[2]Centre for Advanced Process Technology for Urban Resource Recovery (CAPTURE), Particle and Interfacial Technology Group, Ghent University, Coupure Links 653, 9000 Ghent, Belgium

[3]Centre for Membrane Separations, Adsorption, Catalysis and Spectroscopy for Sustainable Solutions (cMACS), KU Leuven, Celestijnenlaan 200F p. o. box 2461, 3001 Leuven, Belgium

[4]Heinz Maier-Leibnitz Zentrum (MLZ), Technische Universität München, Lichtenbergstr. 1, 85748 Garching, Germany and Physik-Department E21, Technische Universität München, James-Franck-Str. 1, 85748 Garching, Germany

[5]Institut für Angewandte Physik und Messtechnik, Universität der Bundeswehr München, Werner-Heisenberg-Weg 39, 85577 Neubiberg, Germany

[6]KWR Watercycle Research Institute, P.O. Box 1072, 3433 PE Nieuwegein, the Netherlands

[7]Mathematical and Statistical Methods - Biometris, Wageningen University and Research, P.O. Box 16, 6700 AA Wageningen, the Netherlands

[8]Facultad del Mar y Medio Ambiente, Universidad Del Pacifico, Ecuador

[9]Lead contact

*Correspondence: malgorzata.roman@wetsus.nl

https://doi.org/10.1016/j.isci.2021.102095

OMPs, legal regulations, and social acceptance. Still, the inherent chemical potential of wastewater can be used in drinking water treatment. For example, the reuse of treated wastewater as a low-salinity stream in ion-exchange membrane (IEM) processes, where wastewater does not mix with the produced drinking water stream, is a promising approach. Treated wastewater can be used as an ion sink in electrodialysis-based pre-desalination of seawater (i.e., as a hybrid seawater desalination process) (Vanoppen et al., 2018; La Cerva et al., 2019) or in reverse electrodialysis (i.e., for green energy generation) (Vermaas et al., 2013; Cipollina and Micale, 2016; Długołecki et al., 2009). The abovementioned use of treated wastewater allows lowering the energy demand of the desalination step. However, in these cases, the potential transport of OMPs through IEMs may pose a risk. This transport is not yet fully understood and requires fundamental investigation.

Previous studies on organics transport in IEM focused mainly on the investigation of the transport of OMPs in a complete IEM stack consisting of alternating cation-exchange membranes (CEM) and anion-exchange membranes (AEM). Thus, only the net transport over the entire stack (i.e., combined transport through AEM and CEM) is reported (Roman et al., 2019; Vanoppen et al., 2015; Banasiak and Schäfer, 2009). On a single-membrane level (i.e., more fundamental study), the ratio of OMP radius to membrane pore radius (and thus diffusive hindrance factors) has been found as the most influential transport parameter of OMPs in IEMs (Ma et al., 2018). However, the experimental fluxes determined on a single-membrane level could not be successfully predicted by the solution-diffusion model (Wijmans and Baker, 2006). Also, a detailed study of the differences between the permeability of AEMs and CEMs toward OMPs is missing. A comprehensive investigation of OMP transport at the single-IEM level is essential to understand the behavior of OMP in an IEM stack. Furthermore, the few existing single-IEM level studies mainly describe the OMP transport in IEMs at high concentrations, where steady-state transport is achieved (Ma et al., 2018; Han et al., 2016). In real-life situations, when using treated wastewater as a source for low-salinity water/ion sink, steady-state conditions may not be achieved at all due to variations in the OMP concentration. These variations are mainly due to weather conditions leading to daily or even hourly disturbance in wastewater composition (Gao et al., 2016; Arola et al., 2017; Zhu and Chen, 2014). In addition, although steric hindrance is described as one of the most significant mechanisms for the partitioning of OMPs in IEMs (Ma et al., 2018; Pronk et al., 2006), it has not been well investigated, because the pore size of IEMs, which can be reflected as the free volume element (FVE) radius of IEMs, has never been reported.

Therefore, the non-steady-state diffusive transport and adsorption kinetics of OMPs in IEMs were investigated in this study. A group of 19 OMPs of different physicochemical characteristics representing major anthropogenic activities (i.e., pesticides, pharmaceuticals, herbicides, food industry, and organic acids) was selected and tested at environmentally relevant concentrations. This group contained six non-charged, seven negatively charged, and six positively charged OMPs. Customized CEMs and AEMs, manufactured from the same polymer but of different thicknesses, were used as a control parameter to describe the transport of OMPs. The dynamic diffusion-adsorption model was used to estimate the adsorption and diffusion coefficients of the OMPs in IEMs. For the first time, positron annihilation lifetime spectroscopy (PALS) was applied to study the FVE radius differences not only between AEMs and CEMs but also as a function of their thicknesses. Thus, this investigation represents a new approach in IEM studies and fills the research gaps in solute transport mechanisms in IEMs. The presented results will contribute to the improved design of next-generation IEMs with more selectivity toward different types of OMPs, and organics in general.

RESULTS AND DISCUSSION

Unraveling similarities in FVE of AEMs and CEMs indicating that differences in their transport are based on interactions developed with OMPs

Wet membrane thickness was selected as a control parameter in the non-steady-state adsorption-diffusion model. Thus, wet thickness values of all membranes used in the experiments were measured. Subsequently, these thickness values were compared with the measured dry membrane thickness values and the membrane swelling degree was calculated. Detailed results are presented in Table S1. The swelling degree of AEMs and CEMs was below 9% for all membrane thicknesses. A clear negative linear dependency between thickness and the swelling degree was found for CEMs (R^2 = 0.97), where thinner membranes were characterized by a higher swelling degree. On the contrary, no visible trend was found for the swelling degree data of AEMs.

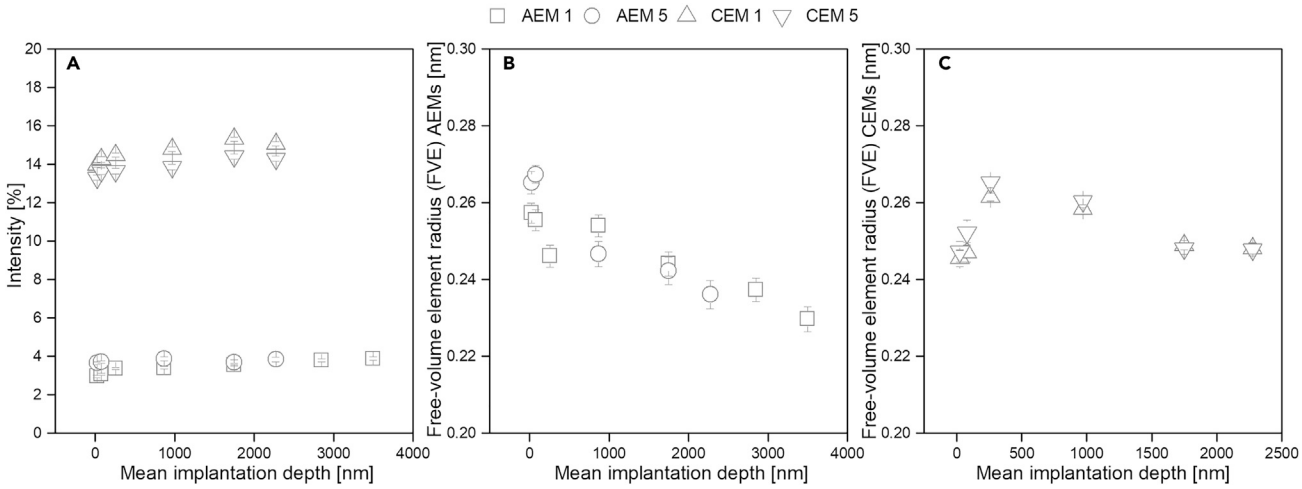

Figure 1. Results of PALS measurements

Intensity (A) and free-volume elements (FVE) radius of AEM (B) and CEM (C) measured at different membrane depths. Error bars indicate standard deviation of the measurement. The presented data correspond to the thinnest and thickest AEMs ($AEM1_{dry}$ = 15.4 ± 0.2 μm, $AEM5_{dry}$ = 87.6 ± 0.3 μm) and CEMs ($CEM1_{dry}$ = 17.7 ± 0.6 μm, $CEM5_{dry}$ = 84.1 ± 3.5 μm).

The size and abundance of the FVE of dry IEMs were characterized using PALS (Figure 1). The average densities of AEMs and CEMs were measured as 1.2 and 0.96 g/cm^3, respectively, and were further used to calculate the mean implantation depths, i.e., depth inside the membrane where the measurement is performed (detailed information is included in the section *Characterization of the membrane polymer structure using PALS* in Transparent methods section of the Supplemental information). PALS analysis was performed at a maximum depth of 4 μm to the membrane surface, i.e., approximately 26.7% and 4.7% of the thickness of AEM5/CEM5 and AEM1/CEM1, respectively. Abbreviations AEM*X* and CEM*X* are explained in the section *Selection of ion exchange membranes* in Transparent methods section of the Supplemental information. The analysis of positron annihilation lifetime spectra revealed that the size distribution of FVEs in IEMs is unimodal, meaning that one main family of FVEs exists in the materials. Their average size (calculated over all measured implementation depths) is not significantly different between AEMs (average FVE_{AEM1} = 0.25 ± 0.007 nm; average FVE_{AEM5} = 0.25 ± 0.008 nm) and CEMs (average FVE_{CEM1} = 0.25 ± 0.01 nm; average FVE_{CEM5} = 0.25 ± 0.01 nm). Furthermore, FVE size was also not dependent on the measurement penetration percentage. The similar swelling degree (below 9%) of AEMs and CEMs indicates that the effect of swelling on their inner structure is comparable between AEMs and CEMs. Thus, in wet membranes (i.e., under the experimental conditions), differences in permeability between AEMs and CEMs toward OMPs result from different IEM-OMP interactions, not from the steric hindrance effect. To the best of our knowledge, the abovementioned results and their scientific relevance have never been reported.

The *o*-Ps intensity was significantly higher for the CEMs (average $intensity_{CEM1}$ = 14.6% ± 0.01%; average $intensity_{CEM5}$ = 13.9% ± 0.02%) than for the AEMs (average $intensity_{AEM1}$ = 3.4% ± 0.01%; average $intensity_{AEM5}$ = 3.8% ± 0.02%) (Figure 1A). This may indicate that more FVEs are present inside the CEMs, compared with the AEMs. Yet, it should be noted that the *o*-Ps intensity is a function of the abundance of FVEs inside the material and the *o*-Ps annihilation probability. The latter is probably different for AEMs and CEMs as they contain different functional groups (Geise et al., 2014; Xie et al., 2011; Pethrick, 1997). When comparing the *o*-Ps intensity obtained for the same membrane type of different thickness, no significant difference was observed. PALS results suggest that the FVE abundance does not change with increased membrane thickness for both AEM and CEM (Figure 1A). When comparing the FVE radii measured at the different implantation depths, AEMs (of both thicknesses, AEM1 and AEM5) were characterized by a slightly larger FVE size at the membrane surface than deeper in the membrane structure (Figure 1B). A clear and negative correlation was found between the FVE radius and the implantation depth for both AEM1 and AEM5, with coefficients of determination of 0.86 and 0.93, respectively. The larger FVEs near the membrane surface could partially reduce the surface resistance of AEMs toward OMP transport. Furthermore, this effect would be more pronounced for thinner AEMs containing a lower quantity of the

denser inner membrane structure. However, those influences are expected to be minor, and their potential impact on the non-steady state transport of OMPs will be further discussed in section *Transport and adsorption of non-charged OMPs*. Contrary to AEMs, CEMs showed a more uniform depth distribution of the FVE radii (Figure 1C).

Remarkably, the FVE radius and intensity of IEMs of the same type but different thickness was similar in magnitude (AEM1 versus AEM5 and CEM1 versus CEM5) (Figures 1B and 1C). The membrane thickness influences neither the size of the FVEs nor their abundance inside the membrane, when measured at the same implantation depth. Furthermore, this suggests that the average degree of polymer crosslinking is comparable between used AEMs and CEMs. This shows how similar those membranes are in their backbone structure and demonstrate that their preparation technique does not significantly influence the membrane polymer density.

Electroneutrality overcomes the diffusive potential of charged OMPs, leading to their complete adsorption in the counter-charged membrane

The behavior of a mixture of 13 charged OMPs of different physicochemical properties in the two-compartment cell was investigated. The list of all OMPs used in the experiment is included in the section *Organic micropollutants used in experiments* (Table S13), and the details of the experimental procedure can be found in the sections *Organic micropollutants and chemical analysis, Selection of ion exchange membranes* (including Table S14), and *OMP diffusion experiments* in the Transparent methods section of the Supplemental information. Experiments were performed after verifying the potential risk of OMP losses due to adsorption in the glass cell (not the membrane) and possible daylight UV degradation. Details of the control experiment are included in the section *OMPs natural degradation and glass adsorption control experiment* (including Figure S7) in Transparent methods section of the Supplemental information.

Charged OMPs were not transported through IEMs but adsorbed onto the membranes (OMPs with an opposite charge compared with the charge of active groups on the membrane) or rejected by membranes (OMPs with the same charge as active groups on the membrane). Atenolol and clofibric acid were selected as model compounds to represent the typical behavior of positively and negatively charged OMPs, respectively (Figure 2). As the trend was the same for all charged OMPs, it was decided to present the results for atenolol and clofibric acid only.

As indicated in our former work, electrostatic interactions are the primary force governing the adsorption of charged OMPs in IEMs (Roman et al., 2019). This type of interaction is long-range, develops fast, and is characterized by the highest strength among non-covalent interactions (Hobza and Müller-Dethlefs, 2010). Adsorption of charged OMPs occurred significantly faster than for non-charged OMPs (discussed further in the section T*ransport and adsorption of non-charged OMPs*). Moreover, in contrast to non-charged OMPs, charged OMPs were fully adsorbed by AEMs and CEMs (100% adsorption). It can be concluded that the adsorption of charged OMPs was entirely based on electrostatic interactions between solute charges and membrane functional groups. Adsorption was observed to be independent of membrane thickness (Figure 2), and membrane capacity (~charge density) was high enough to completely uptake the charged OMPs from the feed solution, including the thinnest membranes (AEM1/CEM1).

It should be noted that at the start of each experiment, OMPs were only present in the feed, whereas the permeate solution contained MilliQ water solely. In such conditions, the membrane free-ions (also referred to as co-ions) are released toward the permeate (Galama et al., 2013). Thus, due to the electroneutrality limitation, the maximum concentration of OMPs in the membranes is equal to the membrane charge density. Owing to the lack of membrane free-ions, OMPs were trapped in the membranes, and their transport toward permeate was below the detection limit. Clearly, electroneutrality overcomes the diffusive potential of charged OMPs, despite their high concentration difference across the membranes.

Transport and adsorption of non-charged OMPs

Type of interactions between the membrane and non-charged OMPs that determine their adsorption and transport

The effect of the membrane thickness on the transport and adsorption of neutral OMPs in IEMs was investigated. The list of all OMPs used in the experiment is included in the section *Organic micropollutants used in experiments* (Table S13), and the details of the experimental procedure can be found in *Organic micropollutants*

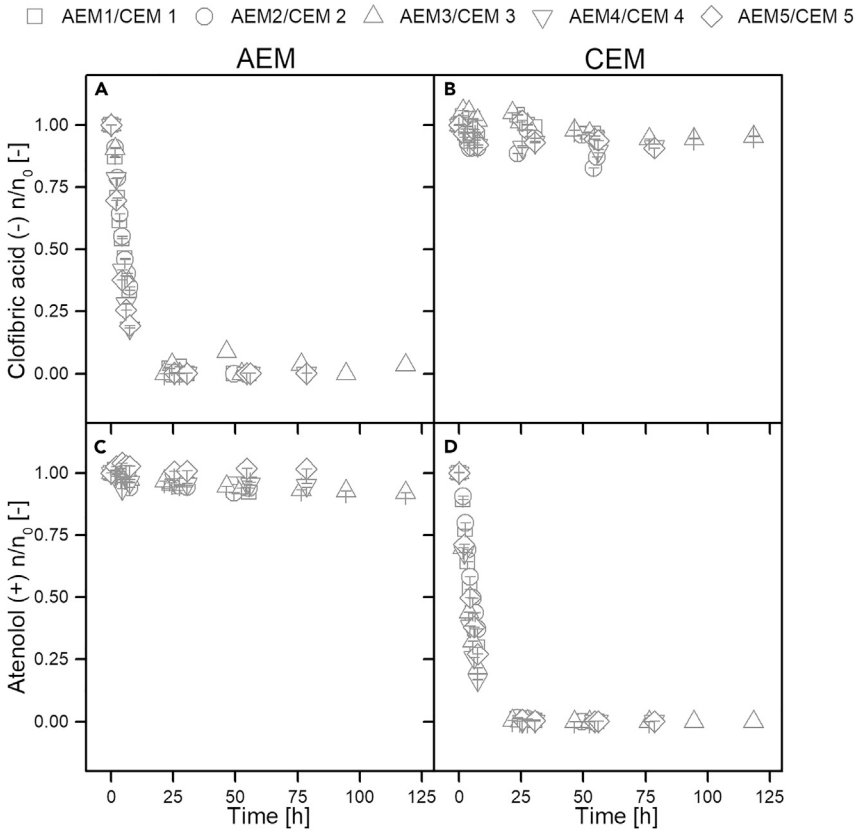

Figure 2. Concentration changes in the experimental time of selected charged organic micropollutants (OMP), shown as the ratio of the number of moles (n) of OMPs measured in the feed solution over the total number of mols (n_0) used

(A) Clofibric acid in experiments with the anion-exchange membrane (AEM).

(B) Clofibric acid in experiments with the cation-exchange membrane (CEM).

(C) Atenolol in experiments with AEM.

(D) Atenolol in experiments with CEM. MilliQ water was used as a permeate. Membrane thicknesses were as follows: $AEM1_{wet}$ = 15.9 ± 3.1 μm, $AEM2_{wet}$ = 33.4 ± 3.8 μm, $AEM3_{wet}$ = 42.3 ± 3.5 μm, $AEM4_{wet}$ = 71 ± 2.8 μm, $AEM5_{wet}$ = 89.6 ± 5.7 μm and $CEM1_{wet}$ = 19 ± 1 μm, $CEM2_{wet}$ = 36.3 ± 1.5 μm, $CEM3_{wet}$ = 51.3 ± 0.6 μm, $CEM4_{wet}$ = 76.7 ± 1.2 μm, $CEM5_{wet}$ = 84.4 ± 3.8 μm. Error bars indicate standard deviation of three independent measurements.

and chemical analysis, Selection of ion exchange membranes (including Table S14), and *OMP diffusion experiments* in the Transparent methods section of the Supplemental information. Experiments were performed after verifying the potential risk of OMP losses due to adsorption in the glass cell (not the membrane) and possible daylight UV degradation. Details of the control experiment are included in the section *OMPs natural degradation and glass adsorption control experiment* (including Figure S7) in Transparent methods section of the Supplemental information. Diffusion experiments were conducted with AEMs, and CEMs were used as a semipermeable barrier between the feed and permeate solutions. Normalized adsorption and transport data of neutral OMPs in AEMs and CEMs are shown in Figures S1 and S2.

In experiments with AEMs and CEMs, the adsorption of OMPs increased with increasing membrane thickness, likely because of the increase in membrane volume and, therefore, the accessible interfacial area between the membrane fibers and OMPs (Figure 3). The adsorption of neutral OMPs was not dependent on the presence of membrane charged groups (i.e., as opposed to charged OMPs). As the adsorption is based on other non-covalent bonds, it depends on the presence of, e.g., hydrogen donor/acceptor sites, hydrocarbon rings, or hydrophobic tails (Faust and Aly, 2013). Figure 3A shows that the predominant type of interaction governing the adsorption of non-charged OMPs onto tested AEMs was the hydrophobic bonding because adsorption increased with the LogD value of OMPs. Adsorption of the strongly hydrophobic diuron was the highest; in contrast, the adsorption of rather hydrophilic caffeine was the lowest.

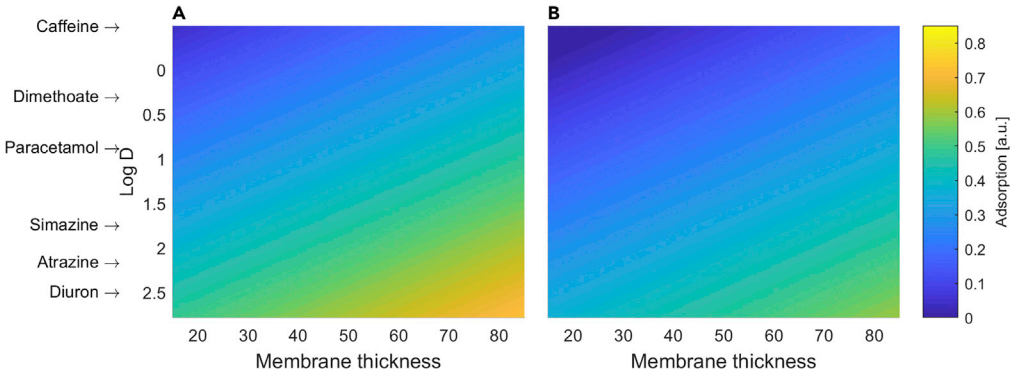

Figure 3. Surface plot representation of the planar regression of normalized adsorption function parameters

Dependency between the normalized adsorption of organic micropollutants (OMP) at 117 h of experiment, membrane thickness, and the hydrophobicity (Log D) of OMPs in anion-exchange membranes (A) and cation-exchange membranes (B) in two-compartment cell experiments. The surface plot represents planar regression of data from Tables S2–S5, with coefficients of determination of 0.59 and 0.75 for (A and B), respectively.

For CEMs, where the adsorption was generally lower than in AEMs, this trend was not observed. However, similar to AEMs, the amount of OMPs adsorbed in CEMs increased with the membrane thickness (Figure 3B). Previous results also emphasized the importance of hydrophobic interactions in the adsorption of non-charged OMPs in IEMs (Roman et al., 2019). However, this is the first study investigating this phenomenon in AEMs and CEMs individually. Remarkably, even in the same type of commercial membranes, interactions between OMPs in AEMs and CEMs can be different, showing the importance of the functional groups.

We also found that the higher the adsorption rate, the faster OMP achieves the membrane equilibrium concentration (C_{eq}), i.e., the membrane reaches its sorptive capacity for a certain OMP (Figures S1 and S2). Also, the faster OMP achieves C_{eq}, the shorter is the time needed to detect OMP in the permeate. This time is hereafter referred to as the diffusion lag time. Beside OMP diffusivity in the membrane, the main reason for the diffusion lag time is the interaction of the OMP with a membrane. In the systems where the adsorption was dependent on the local concentration of solute, i.e., the mass of the solute (OMP) per unit of the membrane was variable, the diffusion lag time was proportional to the thickness and sorptive capacity of the membrane/adsorbent (Flynn and Roseman, 1971; Cooper, 1974; Paul, 1969; Frisch, 1957). In the current work, only diuron in AEM followed this relationship, indicating that only diuron reached C_{eq} in AEM, and thus was further detected in the permeate (Figures S1 and S2). For all other OMPs and IEMs, the diffusion lag time was solely determined by the membrane thickness (Figures S1 and S2). This behavior can be caused by the physicochemical properties of OMPs, i.e., hydrophobicity and size, discussed in detail further in this section.

The total amount of OMP transported through the membrane during the experiment was lower for thicker membranes (Figure 4), likely due to longer diffusion lag time. The transport of OMPs was lower through CEMs compared with AEMs except for caffeine, which was the least transported OMP through AEMs and the most transported through CEMs (Figure 4). According to PALS results, the AEMs and CEMs used in the current study have a comparable FVE. Therefore, the difference between the transport of OMPs in CEMs and AEMs is based on the affinity of OMPs toward the membrane and its functional groups.

Based on the presented data, it can be concluded that the adsorption and transport process of neutral OMPs in IEMs are strongly connected, i.e., adsorption influences diffusion lag time. Furthermore, the more easily OMP establishes membrane saturation (reflected by reaching C_{eq}), the more it is transported (e.g., transport of diuron in AEMs and transport of caffeine in CEMs). Small and hydrophilic caffeine was easily transported through CEMs (less hydrophobic than AEMs). Caffeine is the least hydrophobic compound among the tested OMPs (LogD = -0.55), and CEMs are more hydrophilic than AEMs, which was confirmed by contact angle measurements (Figure S3 and Table S6). Also, higher hydrophobicity of the investigated CEMs is in agreement with the literature, where a higher water transference coefficient was found for the Fumasep CEMs than AEMs (Zlotorowicz et al., 2017). Thus the adsorption rate of caffeine in CEMs was approximately 1,700% higher than in AEMs and quickly achieved C_{eq} (Figures S1 and S2).

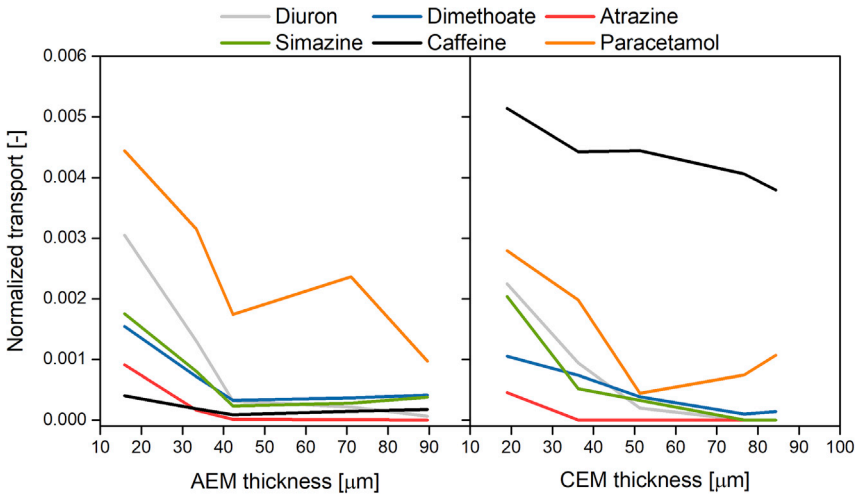

Figure 4. Normalized transport of neutral organic micropollutants in anion-exchange membranes (AEMs) and cation-exchange membranes (CEMs)

Presented data are for all membrane thicknesses, where $AEM1_{wet}$ = 15.9 ± 3.1 μm, $AEM2_{wet}$ = 33.4 ± 3.8 μm, $AEM3_{wet}$ = 42.3 ± 3.5 μm, $AEM4_{wet}$ = 71 ± 2.8 μm, $AEM5_{wet}$ = 89.6 ± 5.7 μm and $CEM1_{wet}$ = 19 ± 1 μm, $CEM2_{wet}$ = 36.3 ± 1.5 [μm], $CEM3_{wet}$ = 51.3 ± 0.6 [μm], $CEM4_{wet}$ = 76.7 ± 1.2 μm, $CEM5_{wet}$ = 84.4 ± 3.8 μm. For the clarity of the plot, error bars are omitted, as their values are below 4% of the average values.

As a result, caffeine was the most intensively transported OMP through CEMs ($n/n_0 = 3.8\times10^{-3}$ - 5.1×10^{-3}, Figure 4), in contrast to AEMs, wherein it was practically the least transported ($n/n_0 = 0.1\times10^{-3}$- 0.4×10^{-3}, Figure 4). Unlike caffeine, diuron is most hydrophobic (LogD = 2.53) among the tested OMPs, and its adsorption rate in CEMs was approximately 65% lower than in AEMs. Thus, hydrophobicity significantly increased the diffusion lag time of diuron in CEMs (Figures S1 and S2), preventing its transport through the two thickest membranes (CEM4 and CEM5) (Figure 4).

Next to the hydrophobicity of OMPs, steric hindrance had a major impact on the OMP transport. As we aim to compare the molecular dimension (steric hindrance) with FVE size, we found that the molecular radius is the most suitable parameter to use. The average molecular radius of tested OMPs calculated from their van der Waals volumes are as follows: r_{diuron} = 0.36 nm, $r_{dimethoate}$ = 0.35 nm, $r_{atrazine}$ = 0.36 nm, $r_{simazine}$ = 0.35 nm, $r_{caffeine}$ = 0.34 nm, and $r_{paracetamol}$ = 0.32 nm. Noticeably, the studied OMPs were characterized by a similar estimated molecular dimension. Interestingly, the FVE (~0.25 nm) determined with PALS is smaller than the above-presented molecular dimensions. However, after considering the swelling degree to be below 9% (Table S1) for all membranes and their thicknesses, the calculated FVE radius was approximately 0.28 nm. Also, this value is an average value over the whole implantation depth measurements. Therefore, this result indicates that the dimensions of OMPs are in the same order of magnitude as the FVE size of the selected IEMs. Considering this, even minor differences in the geometry of OMPs might have an impact on their transport properties. Therefore, this would be a plausible reason why paracetamol penetrates membranes more easily in AEMs than other OMPs. PALS results show that AEMs were characterized by a slightly more open structure at the membrane surface. Possibly these open-ended FVEs could slightly decrease AEM surface resistance, as also reported elsewhere (Sarapulova et al., 2019). However, these differences are small, and further confirmation would require more research effort, including experiments with asymmetric membranes.

Simazine and atrazine behaved differently than the OMPs explained earlier. Both compounds were the least transported through IEMs (Figure 4), although showing relatively high hydrophobicity (LogD between 1.78 and 2.2). Atrazine and simazine are characterized by the highest hydrogen donor/acceptor count (both 7), which is significantly higher compared with the other tested OMPs (between 2 and 4). Possibly, the adsorption of atrazine and simazine was assisted by strong hydrogen bonds, which were even more significant in the more hydrophilic CEMs. Therefore, despite the fast adsorption of simazine and atrazine and achieving C_{eq}, the adsorption was strong enough to significantly decrease their transport (Figure 4).

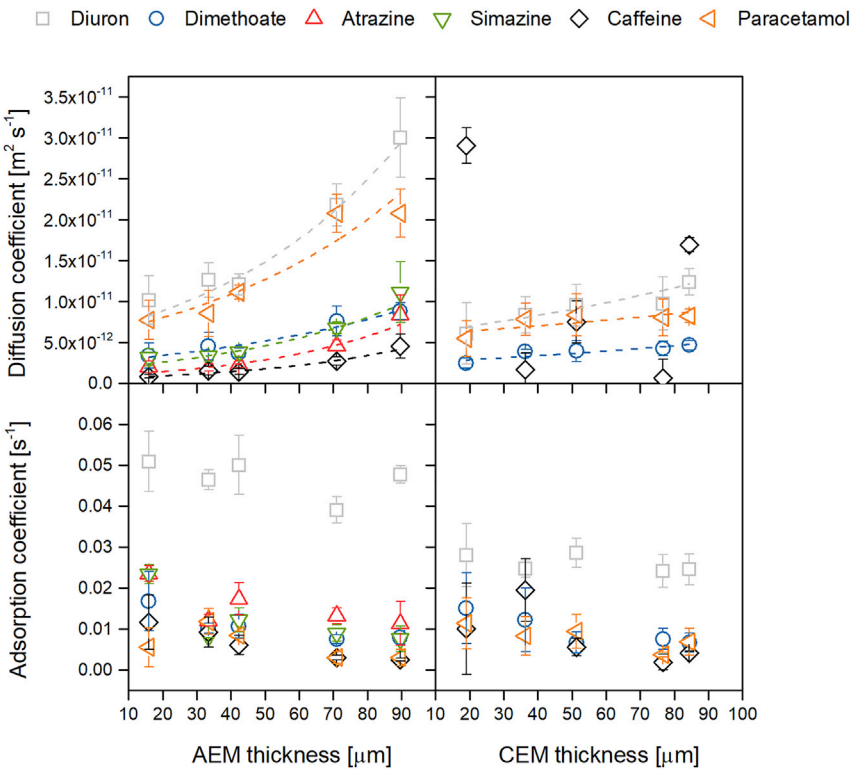

Figure 5. Diffusion and adsorption coefficients for the transport of organic micropollutants through anion-exchange membranes (AEMs) and cation-exchange membranes (CEMs) at different membrane thicknesses.
For figure clarity, standard errors are shown for the estimated coefficients only, whereas error on measured thicknesses is omitted. Dashed lines indicate the regression (exponential) fit.

The identification of adsorption-transport mechanisms of neutral OMPs, and learning about exceptions such as atrazine and simazine, creates the possibility to reconsider potential membrane design to limit membrane permeability toward OMPs. It was shown that thicker and denser membranes might contribute to limiting the transport of OMPs. However, increasing membrane thickness would also increase membrane electrical resistance. The proper selection of those membrane parameters would be a trade-off solution, evaluated based on the needs of the specific IEMs system.

Surface resistance increases the diffusion coefficient along with membrane thickness in the dynamic diffusion-adsorption model

Diffusion and adsorption coefficients describing the transport of neutral OMPs through AEMs and CEMs (all thicknesses) were estimated with the non-steady-state diffusion-adsorption model. Details of model description and determination of diffusion and adsorption coefficients are included in the section *Dynamic diffusion-adsorption model for determination of transport coefficients of organic micropollutants in IEM* (including Figures S8 and S9) in the Transparent methods section of the Supplemental information. The obtained coefficients are presented in Figure 5, while the detailed values of the coefficients with their uncertainties are in Tables S7–S10.

An exponential dependency ($y = a \cdot \exp(b \cdot x)$) between the diffusion coefficient and membrane thickness was found for AEMs and CEMs (Figure 5). In CEMs, caffeine did not follow the exponential trend probably because of its hydrophilicity, which significantly changed the nature of caffeine-CEM surface interactions. Data of simazine and atrazine are not included due to lack of transport of these compounds through the CEMs. The lack of transport can be explained by the pH drop in parts of the experiments (Tables S11 and S12). This change in pH led to the ionization of simazine and atrazine (not affecting any other OMPs) and resulted in the adsorption of these compounds onto CEMs (section *Electroneutrality overcomes the diffusive potential of charged OMPs, leading to their complete adsorption in the counter-charged membrane*).

From the results presented in Figure 5, the diffusion coefficient increased with AEM and CEM membrane thickness. By definition, the diffusion coefficient is a measure of rate at which molecule transports in a certain material or media (Crank, 1979; Cooper, 1974). Therefore, it can be expected that in IEMs, made from the same polymer, the diffusion coefficient will be constant for all thicknesses. The potential effect of the microstructural differences between different thicknesses of the membranes was validated using PALS, which indicated that membranes of different thicknesses were considerably similar in FVE radius and intensity (Figure 1). Thus, the increase in the diffusion coefficient for the thicker membranes is not an effect of such differences, e.g., a more open structure of thicker membranes. The most probable reason why the determined diffusion coefficients are thickness-dependent is different interactions between species at the surface and in the bulk of the layer. It is known that surfaces are characterized by higher energy than the bulk of the material (Packham, 2003). Thus, surfaces create a barrier of high resistance. This phenomenon is more prominent in a thinner membrane, as the ratio between bulk and surface energies is the lowest. These findings are in agreement with other previous studies mentioning the influence of the layer thickness of diffusive material on the diffusion coefficient of transported species (Buss et al., 2015; Nath, 2014; Park and Aluru, 2010). Another potential mechanism responsible for the dependency of the diffusion coefficient on the membrane thickness is the double transport mechanism (Galama et al., 2013, 2016b), which covers the surface diffusion along with the membrane polymers and transport through the solvent in the FVE. As the diffusion along the polymer surface could occur faster than the diffusion in the solvent in the FVEs, the contribution of the surface polymer diffusion increases along with the membrane thickness. Therefore, the measured diffusion coefficients could be higher in thicker membranes. More thorough research, specifically with more extended experimental duration to study the transition from non-equilibrium to steady state, is necessary to confirm these key observations.

The regression parameter *b*, describing the growth of the diffusion coefficient versus thickness (Figure 5), was found as independent of the OMPs, but dependent on the type of membrane (Figures S4–S6). A 2-fold higher growth of diffusion coefficient was observed in AEMs ($b = 18.393 \pm 1536$) than in CEMs ($b = 8394 \pm 879$). Most likely, the differences between the parameter *b* in AEMs and CEMs are due to their different chemical compositions, and thus polymer structure (described in the section *Type of interactions between the membrane and non-charged OMPs that determine their adsorption and transport*). Nevertheless, this hypothesis could not be confirmed with PALS results.

The second regression parameter *a* describes the diffusion coefficient for a hypothetical infinitely thin membrane. In theory, this parameter corresponds to the diffusion coefficient in water; however, it is found to be substantially lower. For example, the diffusion coefficient of paracetamol in water is around 140-fold higher than the estimated parameter *a* (759×10^{-12} versus 6.5×10^{-12} m^2 s^{-1}, Figures S4–S6). Thus, it can be concluded that the difference between the value of the diffusion coefficient in water and the estimated parameter *a* is a measure of the surface effect on the diffusion. The difference between estimated parameter *a* and diffusion coefficient in water is different for each OMP (Figures S4–S6). In AEMs, the correlation analysis indicated that the hydrophobicity of OMPs is the responsible parameter for the surface resistance (Pearson's $R = -0.993$, p values < 0.05). This confirms that hydrophobic interactions play a significant role in the adsorption of OMPs in AEMs and is in agreement with the description of adsorption and transport mechanisms described in the section *Type of interactions between the membrane and non-charged OMPs that determine their adsorption and transport*. In CEMs, the correlation analysis indicated that the topological polar surface of OMPs is the responsible parameter for the surface resistance (Pearson's $R = 0.970$, p value < 0.05). The topological polar surface area is the area of its van der Waals surface arising from oxygen or nitrogen atoms, or hydrogen atoms attached to oxygen or nitrogen atoms. As such, it is a measure of the compound's capacity to form hydrogen bonds (Roman et al., 2019; Clark, 1999). Probably, the formation of hydrogen bonds at the membrane surface is responsible for limiting the transport of OMPs in the investigated CEMs.

In contrast to diffusion coefficients, adsorption coefficients were found independent of the membrane thickness in AEMs and CEMs (Figure 5). The adsorption coefficient corresponds to the rate of surface interactions between OMP and the membrane; thus, it is similar in physical meaning to the rates described in the section *Type of interactions between the membrane and non-charged OMPs that determine their adsorption and transport*. A strong correlation between the average adsorption coefficient and LogD was found (Pearson's $R = 0.904$, p-values < 0.05), which reflects a strong dependency of OMPs' adsorption in AEMs on the hydrophobic bonding.

Limitations of the study

In this study, we performed a comprehensive investigation of OMPs' transport through a single IEM under non-steady-state conditions. As so little is known about the fundamentals of the behavior of OMPs in IEMs, it was decided to design experiments wherein the transport was investigated at a single-membrane level, with one major driving force, i.e., diffusion. Thus, to limit the influence of the convection and electromigration, no inorganic salts were added and no external electrical potential was applied. This created an opportunity for a detailed study of the transport of the non-charged OMPs, although only adsorption of charged OMPs was observed. That is why the fundamental study of the transport of charged OMPs still requires further research, e.g., experiments involving the application of different, monovalent and multivalent, inorganic salts in two-compartment cells. Inorganic salts' presence eliminates the limiting effect of electroneutrality in the transport of charged OMPs through IEMs. Furthermore, due to the lack of transport of charged OMPs, a detailed investigation of ion-exchange capacity (IEC) for each membrane thickness was not performed. As explained in the section *Electroneutrality overcomes the diffusive potential of charged OMPs, leading to their complete adsorption in the counter-charged membrane*, the adsorption of charged OMPs was entirely based on electrostatic interactions between solute charges and membrane functional groups. Thus, a comparison of the charged OMPs' transport data with IECs could verify the effect of membrane saturation on the transport of charged OMPs. However, results obtained using PALS verified that different thicknesses of membranes from the same polymer are uniform in their properties. PALS signal intensity is also dependent on the membrane chemistry, i.e., the presence of the ion-exchange groups. Based on the presented results (Figure 1A), we concluded that chemical properties are the same for different membranes' thicknesses, as the intensity does not vary between AEM1/AEM5 and CEM1/CEM5. Thus, we can expect that IECs also do not vary significantly between membranes. Unlike IECs, we expect that membrane electrical resistance increases with membrane thickness. Next to the internal membrane parameters, we think that the membrane's surface resistances also determine the electrical resistance. A commonly used method to measure the membrane's electrical resistance, i.e., applying a six-compartment cell, is not suitable to measure thin membranes (Długołęcki et al., 2010; Galama et al., 2016a). A high error is caused by the imprecise alignment of Haber-Luggin capillaries, the fluctuation of membranes caused by the electrolytes' flow inside the cell, and a lack of differentiation in resistance between the investigated membrane and the surrounding solution. Developing a precise method to measure membrane resistance is crucial to report the membrane's resistance thickness.

In this study, we investigated one type of membrane at different thicknesses (S10) manufactured from the same polymer (stock) solution. We evidenced that the interactions between OMPs and the membrane material determine the OMP transport, whereas the interaction depends on the physicochemical parameters of OMPs. We found that the adsorption and transport process of neutral OMPs in IEMs are strongly dependent on each other, i.e., adsorption influences the diffusion lag time. Furthermore, the easier OMPs reach membrane saturation (reflected by obtaining C_{eq}), the more OMPs are transported. We strongly believe that the presented conclusions are universal and valid also for different types of membranes. Of course, certain differences, e.g., the time of obtaining membrane saturation, are different depending on the membrane parameters.

Resource availability

Lead contact

Further information and requests for resources should be directed to and will be fulfilled by the Lead Contact, Malgorzata Roman (malgorzata.roman@wetsus.nl).

Materials availability

This study did not use any special materials.

Data and code availability

This study did not generate any datasets.

METHODS

All methods can be found in the accompanying Transparent Methods supplemental file.

SUPPLEMENTAL INFORMATION

Supplemental information can be found online at https://doi.org/10.1016/j.isci.2021.102095.

ACKNOWLEDGMENTS

This work was performed in the cooperation framework of Wetsus, the European Center of Excellence for Sustainable Water Technology (www.wetsus.eu). Wetsus is co-funded by the Dutch Ministry of Economic Affairs and Ministry of Infrastructure and the Environment, the Province of Fryslân, and the Northern Netherlands Provinces. This project has also received funding from the European Union's Horizon 2020 research under grant agreement No 685579 (www.revivedwater.eu). The authors thank Dr. Bas Wols for his support and discussions regarding the adsorption of organic micropollutants. PALS experiments were performed at the NEPOMUC PLEPS instrument operated by FRM-II at the Heinz Maier Leibnitz Zentrum (MLZ) in Garching, Germany. The authors would like to thank the participants of the research theme "Blue Energy" for their input, suggestions, and financial support. R.V. thanks Research Foundation Flanders (FWO) for her SB-PhD fellowship (1S00917N). Finally, the authors would like to express their gratitude to the Wetsus technical support team.

AUTHOR CONTRIBUTIONS

Conceptualization, M.R. and M.V.; Methodology, M.R., P.R., and M.V.; Software, P.R. and K.K.; Formal Analysis, M.R., P.R., and K.K.; Investigation, M.R., R.V., M.D., and W.E.; Writing – Original Draft, M.R.; Writing – Review & Editing, M.R., P.R., L.G., J.P., E.C., and A.V.; Supervision, A.V., E.C., J.P., K.K., and I.V.

DECLARATION OF INTERESTS

The authors declare no competing interests.

Received: September 28, 2020
Revised: December 11, 2020
Accepted: January 15, 2021
Published: February 19, 2021

REFERENCES

Arola, K., Hatakka, H., Mänttäri, M., and Kallioinen, M. (2017). Novel process concept alternatives for improved removal of micropollutants in wastewater treatment. Sep. Purif. Technol. *186*, 333–341.

Banasiak, L.J., and Schäfer, A.I. (2009). Removal of inorganic trace contaminants by electrodialysis in a remote Australian community. Desalination *248*, 48–57.

Bixio, D., Thoeye, C., De Koning, J., Joksimovic, D., Savic, D., Wintgens, T., and Melin, T. (2006). Wastewater reuse in europe. Desalination *187*, 89–101.

Bolong, N., Ismail, A., Salim, M.R., and Matsuura, T. (2009). A review of the effects of emerging contaminants in wastewater and options for their removal. Desalination *239*, 229–246.

Buss, F., Göcke, J., Scharfer, P., and Schabel, W. (2015). From micro to nano thin polymer layers: thickness and concentration dependence of sorption and the solvent diffusion coefficient. Macromolecules *48*, 8285–8293.

Cipollina, A., and Micale, G. (2016). Sustainable Energy from Salinity Gradients (Woodhead Publishing).

Clark, D.E. (1999). Rapid calculation of polar molecular surface area and its application to the prediction of transport phenomena. 1. Prediction of intestinal absorption. J. Pharm. Sci. *88*, 807–814.

Cooper, E.R. (1974). Effect of adsorption on membrane diffusion. J. Colloid Interfaces Sci. *48*, 516–517.

Crank, J. (1979). The Mathematics of Diffusion (Oxford university press).

Daughton, C.G., and Ternes, T.A. (1999). Pharmaceuticals and personal care products in the environment: agents of subtle change? Environ. Health Perspect. *107*, 907–938.

Deblonde, T., Cossu-Leguille, C., and Hartemann, P. (2011). Emerging pollutants in wastewater: a review of the literature. Int. J. Hyg. Environ. Health *214*, 442–448.

DługołeCki, P., Gambier, A., Nijmeijer, K., and Wessling, M. (2009). Practical potential of reverse electrodialysis as process for sustainable energy generation. Environ. Sci. Technol. *43*, 6888–6894.

Długołęcki, P., Ogonowski, P., Metz, S.J., Saakes, M., Nijmeijer, K., and Wessling, M. (2010). On the resistances of membrane, diffusion boundary layer and double layer in ion exchange membrane transport. J. Membr. Sci. *349*, 369–379.

Faust, S.D., and Aly, O.M. (2013). Adsorption Processes for Water Treatment (Elsevier).

Flynn, G., and Roseman, T. (1971). Membrane diffusion II: influence of physical adsorption on molecular flux through heterogeneous dimethylpolysiloxane barriers. J. Pharm. Sci. *60*, 1788–1796.

Frisch, H.L. (1957). The time lag in diffusion. J. Phys. Chem. *61*, 93–95.

Gabarrón, S., Gernjak, W., Valero, F., Barceló, A., Petrovic, M., and Rodríguez-Roda, I. (2016). Evaluation of emerging contaminants in a drinking water treatment plant using electrodialysis reversal technology. J. Hazard. Mater. *309*, 192–201.

Galama, A., Hoog, N., and Yntema, D. (2016a). Method for determining ion exchange membrane resistance for electrodialysis systems. Desalination *380*, 1–11.

Galama, A., Post, J., Hamelers, H., Nikonenko, V., and Biesheuvel, P. (2016b). On the origin of the membrane potential arising across densely charged ion exchange membranes: how well does the Teorell-Meyer-Sievers theory work? J. Membr. Sci. Res. *2*, 128–140.

Galama, A., Post, J., Stuart, M.C., and Biesheuvel, P. (2013). Validity of the Boltzmann equation to describe Donnan equilibrium at the membrane–solution interface. J. Membr. Sci. *442*, 131–139.

Gao, J., Huang, J., Chen, W., Wang, B., Wang, Y., Deng, S., and Yu, G. (2016). Fate and removal of typical pharmaceutical and personal care products in a wastewater treatment plant from Beijing: a mass balance study. Front. Environ. Sci. Eng. *10*, 491–501.

Geise, G.M., Doherty, C.M., Hill, A.J., Freeman, B.D., and Paul, D.R. (2014). Free volume characterization of sulfonated styrenic pentablock copolymers using positron

annihilation lifetime spectroscopy. J. Membr. Sci. *453*, 425–434.

Grant, S.B., Saphores, J.-D., Feldman, D.L., Hamilton, A.J., Fletcher, T.D., Cook, P.L., Stewardson, M., Sanders, B.F., Levin, L.A., and Ambrose, R.F. (2012). Taking the "waste" out of "wastewater" for human water security and ecosystem sustainability. Science *337*, 681–686.

Han, L., Galier, S., and Roux-De Balmann, H. (2016). Transfer of neutral organic solutes during desalination by electrodialysis: influence of the salt composition. J. Membr. Sci. *511*, 207–218.

Hobza, P., and Müller-Dethlefs, K. (2010). Non-covalent Interactions: Theory and Experiment (Royal Society of Chemistry).

Jobling, S., Nolan, M., Tyler, C.R., Brighty, G., and Sumpter, J.P. (1998). Widespread sexual disruption in wild fish. Environ. Sci. Technol. *32*, 2498–2506.

Jones, O.A., Voulvoulis, N., and Lester, J.N. (2003). Potential impact of pharmaceuticals on environmental health. Bull. World Health Organ. *81*, 768–769.

La Cerva, M., Gurreri, L., Cipollina, A., Tamburini, A., Ciofalo, M., and Micale, G. (2019). Modelling and cost analysis of hybrid systems for seawater desalination: electromembrane pre-treatments for Reverse Osmosis. Desalination *467*, 175–195.

Ma, L., Gutierrez, L., Vanoppen, M., Aubry, C., and Verliefde, A. (2018). Transport of uncharged organics in ion-exchange membranes: experimental validation of the solution-diffusion model. J. Membr. Sci. *564*, 773–781.

McKinlay, R., Plant, J., Bell, J., and Voulvoulis, N. (2008). Endocrine disrupting pesticides: implications for risk assessment. Environ. Int. *34*, 168–183.

Murray, K.E., Thomas, S.M., and Bodour, A.A. (2010). Prioritizing research for trace pollutants and emerging contaminants in the freshwater environment. Environ. Pollut. *158*, 3462–3471.

Nath, S.D. (2014). On the thickness-dependent diffusion coefficient of perfluoropolyether lubricants on a thin diamond-like film. Appl. Phys. A *117*, 857–870.

Ohe, T., Watanabe, T., and Wakabayashi, K. (2004). Mutagens in surface waters: a review. Mutat. Res./Rev. Mutat. Res. *567*, 109–149.

Osenbrück, K., Gläser, H.-R., Knöller, K., Weise, S.M., Möder, M., Wennrich, R., Schirmer, M., Reinstorf, F., Busch, W., and Strauch, G. (2007). Sources and transport of selected organic micropollutants in urban groundwater underlying the city of Halle (Saale), Germany. Water Res. *41*, 3259–3270.

Packham, D.E. (2003). Surface energy, surface topography and adhesion. Int. J. Adhes. Adhes. *23*, 437–448.

Park, J.H., and Aluru, N.R. (2010). Water film thickness-dependent conformation and diffusion of single-strand DNA on poly (ethylene glycol)-silane surface. Appl. Phys. Lett. *96*, 123703.

Paul, D. (1969). Effect of immobilizing adsorption on the diffusion time lag. J. Polym. Sci. *7*, 1811–1818.

Pethrick, R.A. (1997). Positron annihilation—a probe for nanoscale voids and free volume? Prog. Polym. Sci. *22*, 1–47.

Pronk, W., Biebow, M., and Boller, M. (2006). Electrodialysis for recovering salts from a urine solution containing micropollutants. Environ. Sci. Technol. *40*, 2414–2420.

Richardson, S.D., and Ternes, T.A. (2014). Water analysis: emerging contaminants and current issues. Anal. Chem. *86*, 2813–2848.

Roman, M., Van Dijk, L., Gutierrez, L., Vanoppen, M., Post, J., Wols, B., Cornelissen, E., and Verliefde, A. (2019). Key physicochemical characteristics governing organic micropollutant adsorption and transport in ion-exchange membranes during reverse electrodialysis. Desalination *468*, 114084.

Sarapulova, V., Shkorkina, I., Mareev, S., Pismenskaya, N., Kononenko, N., Larchet, C., Dammak, L., and Nikonenko, V. (2019). Transport characteristics of fujifilm ion-exchange membranes as compared to homogeneous membranes АМЧ and СМЧ and to heterogeneous membranes MK-40 and MA-41. Membranes *9*, 84.

Schwarzenbach, R.P., Escher, B.I., Fenner, K., Hofstetter, T.B., Johnson, C.A., Von Gunten, U., and Wehrli, B. (2006). The challenge of micropollutants in aquatic systems. Science *313*, 1072–1077.

Sirés, I., and Brillas, E. (2012). Remediation of water pollution caused by pharmaceutical residues based on electrochemical separation and degradation technologies: a review. Environ. Int. *40*, 212–229.

Sui, Q., Cao, X., Lu, S., Zhao, W., Qiu, Z., and Yu, G. (2015). Occurrence, sources and fate of pharmaceuticals and personal care products in the groundwater: a review. Emerg. Contam. *1*, 14–24.

Tang, C.Y., Yang, Z., Guo, H., Wen, J.J., Nghiem, L.D., and Cornelissen, E. (2018). Potable Water Reuse through Advanced Membrane Technology (ACS Publications).

Tang, J.Y., Mccarty, S., Glenn, E., Neale, P.A., Warne, M.S.J., and Escher, B.I. (2013). Mixture effects of organic micropollutants present in water: towards the development of effect-based water quality trigger values for baseline toxicity. Water Res. *47*, 3300–3314.

Vanoppen, M., Bakelants, A.F., Gaublomme, D., Schoutteten, K.V., Bussche, J.V., Vanhaecke, L., and Verliefde, A.R. (2015). Properties governing the transport of trace organic contaminants through ion-exchange membranes. Environ. Sci. Technol. *49*, 489–497.

Vanoppen, M., Blandin, G., Derese, S., Le Clech, P., Post, J., and Verliefde, A.R.D. (2016). Salinity Gradient Power and desalination. Salinity Gradient Power and Desalination. Sustainable Energy from Salinity Gradients (Woodhead publishing).

Vanoppen, M., Criel, E., Walpot, G., Vermaas, D.A., and Verliefde, A. (2018). Assisted reverse electrodialysis—principles, mechanisms, and potential. Npj Clean. Water *1*, 9.

Verliefde, A.R.D. (2008). Rejection of Organic Micropollutants by High Pressure Membranes (NF/RO) (TU Delft, Delft University of Technology).

Vermaas, D.A., Veerman, J., Yip, N.Y., Elimelech, M., Saakes, M., and Nijmeijer, K. (2013). High efficiency in energy generation from salinity gradients with reverse electrodialysis. ACS Sustain. Chem. Eng. *1*, 1295–1302.

Water, U. (2009). The United Nations World Water Development Report 3–Water in a Changing World (United Nations Educational Scientific and Cultural Organization).

Wijmans, J.G., and Baker, R.W. (2006). The solution-diffusion model: a unified approach to membrane permeation. In Materials Science of Membranes for Gas and Vapor Separation, Y. Yampolskii, I. Pinnau, and B. Freeman, eds. (John Wiley & Sons), pp. 159–189.

Xie, W., Ju, H., Geise, G.M., Freeman, B.D., Mardel, J.I., Hill, A.J., and Mcgrath, J.E. (2011). Effect of free volume on water and salt transport properties in directly copolymerized disulfonated poly (arylene ether sulfone) random copolymers. Macromolecules *44*, 4428–4438.

Zhu, S., and Chen, H. (2014). The fate and risk of selected pharmaceutical and personal care products in wastewater treatment plants and a pilot-scale multistage constructed wetland system. Environ. Sci. Pollut. Res. *21*, 1466–1479.

Zlotorowicz, A., Strand, R.V., Burheim, O.S., Wilhelmsen, Ø., and Kjelstrup, S. (2017). The permselectivity and water transference number of ion exchange membranes in reverse electrodialysis. J. Membr. Sci. *523*, 402–408.

iScience, Volume *24*

Supplemental Information

Non-steady diffusion and adsorption of organic micropollutants in ion-exchange membranes: effect of the membrane thickness

Malgorzata Roman, Pawel Roman, Rhea Verbeke, Leonardo Gutierrez, Marjolein Vanoppen, Marcel Dickmann, Werner Egger, Ivo Vankelecom, Jan Post, Emile Cornelissen, Karel Keesman, and Arne Verliefde

Supplemental data items

Wet and dry membrane thicknesses measured by an optical microscope

Table S1. Average thicknesses of wet and dry IEMs used in experiments, with calculated membrane swelling. Related to Figure 1-5 and discussed in the manuscript's 2.1. section.

Membrane	Average dry thickness [µm]	StDev [-]	Average wet thickness [µm]	StDev [-]	% swelling	swelling error
AEM 1	15.4	0.2	15.9	3.1	3.2	0.111
AEM 2	30.9	1.8	33.4	3.8	8.1	0.082
AEM 3	41.4	0.2	42.3	3.5	2.2	0.044
AEM 4	70.7	0.8	71	2.8	0.4	0.026
AEM 5	87.6	0.3	89.6	5.7	2.3	0.027
CEM 1	17.7	0.6	19	1	7.5	0.063
CEM 2	34.7	1.2	36.3	1.5	4.8	0.048
CEM 3	49.7	0.6	51.3	0.6	3.4	0.019
CEM 4	75.3	1.2	76.7	1.2	1.8	0.021
CEM 5	84.1	3.5	84.4	3.8	0.4	0.048

Results of diffusion experiments with AEMs and CEMs used as a semipermeable barrier between feed and permeate solutions

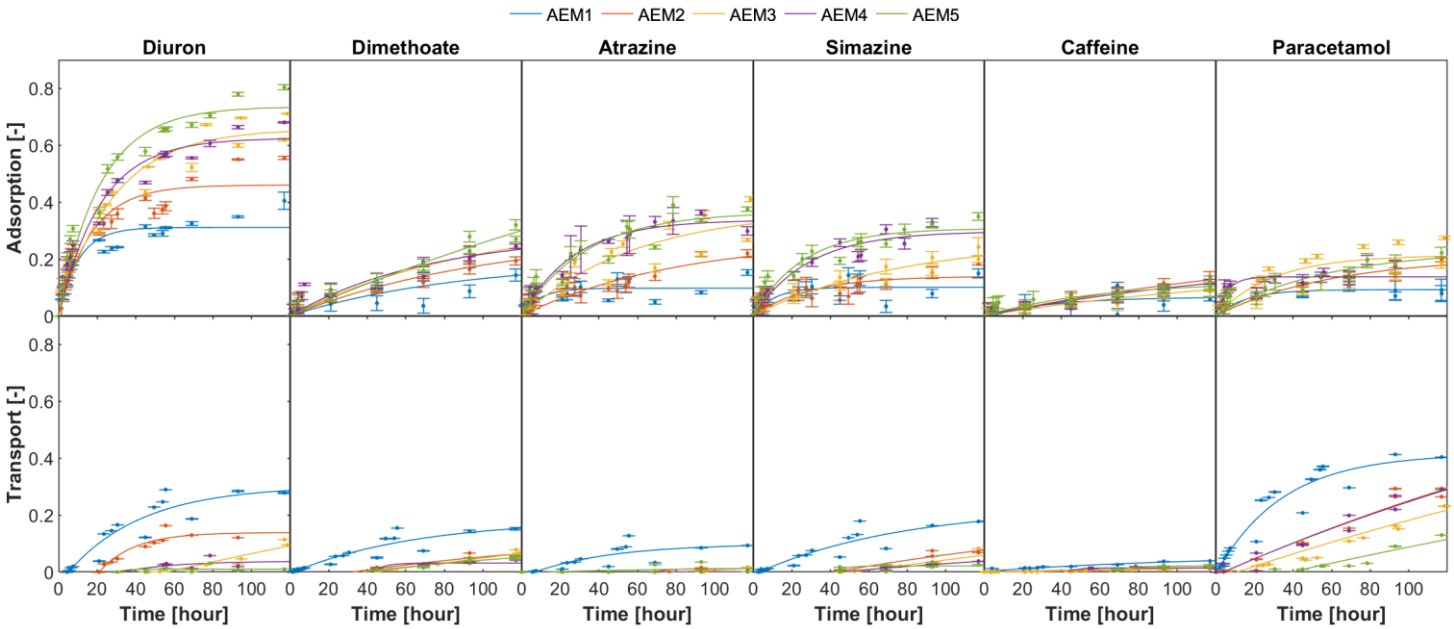

Figure S1. Normalized adsorption and transport of non-charged organic micropollutants in diffusion experiments with anion exchange membranes. Presented data are for all membrane thicknesses, where $AEM1_{wet}$ = 15.9 ± 3.1 [µm], $AEM2_{wet}$ = 33.4 ± 3.8 [µm], $AEM3_{wet}$ = 42.3 ± 3.5 [µm], $AEM4_{wet}$ = 71 ± 2.8 [µm], $AEM5_{wet}$ = 89.6 ± 5.7 [µm]. Each point represents an average of measurements from three independent experiments. Lines indicate best-fitting function, where adsorption follows first-order kinetics. The coefficient of determination for each fit is included in Table S2–S5. Related to Figure 3 and 4 and discussed in the manuscript's 2.3.1 section.

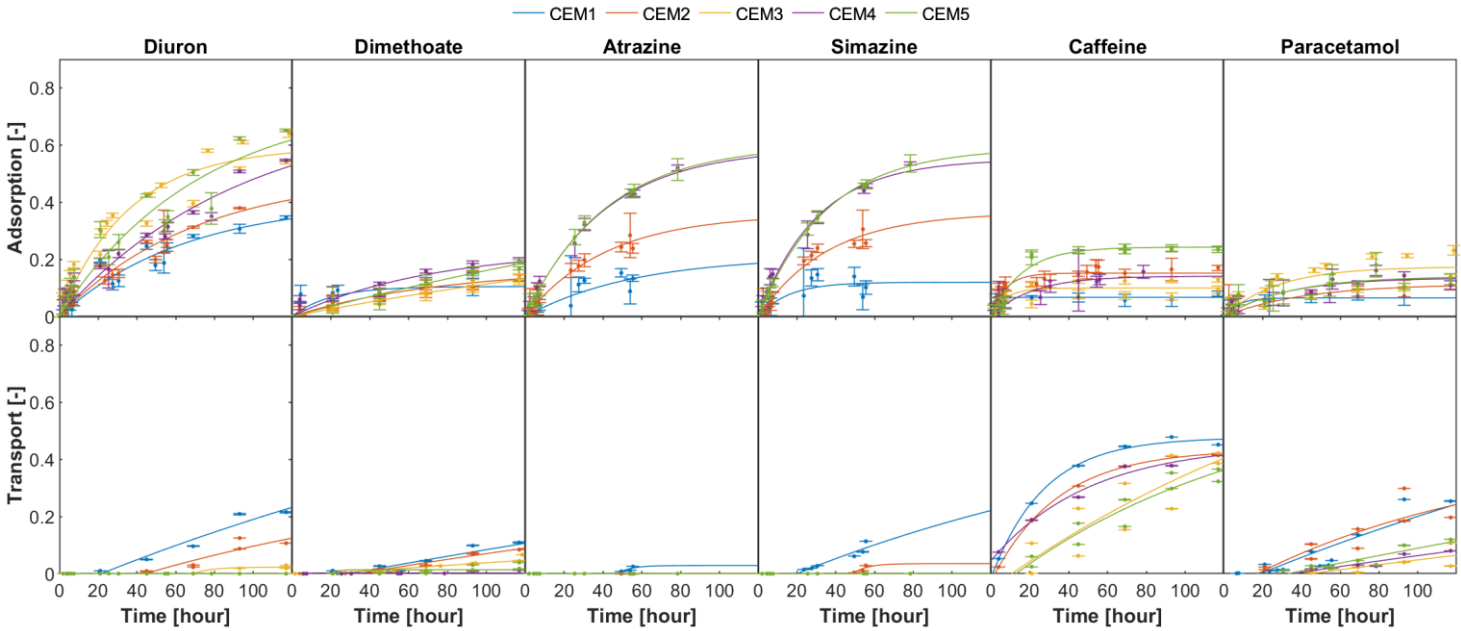

Figure S2. Normalized adsorption and transport of neutral organic micropollutants in diffusion experiments with cation exchange membranes. Presented data are for all membrane thicknesses, where $CEM1_{wet}$ = 19 ± 1 [µm], $CEM2_{wet}$ = 36.3 ± 1.5 [µm], $CEM3_{wet}$ = 51.3 ± 0.6 [µm], $CEM4_{wet}$ = 76.7 ± 1.2 [µm], $CEM5_{wet}$ = 84.4 ± 3.8 [µm]. Each point represents an average of measurements from three independent experiments. Lines indicate best-fitting function, where adsorption follows first-order kinetics. The coefficient of determination for each fit is included in Table S2–S5. Related to Figure 3 and 4 and discussed in the manuscript's 2.3.1 section.

Fitting parameters of normalized adsorption and transport function

Table S2. Normalized adsorption function parameters and their coefficients of determination for anion exchange membranes. Related to Figure 3.

		R^2	a	b	c
Diuron	AEM 1	0.977	-0.311	0.097	0.312
Diuron	AEM 2	0.972	-0.459	0.059	0.461
Diuron	AEM 3	0.986	-0.656	0.036	0.658
Diuron	AEM 4	0.989	-0.624	0.046	0.625
Diuron	AEM 5	0.988	-0.734	0.046	0.736
Dimethoate	AEM 1	0.847	-0.193	0.011	0.194
Dimethoate	AEM 2	0.978	-0.295	0.009	0.295
Dimethoate	AEM 3	0.966	-0.347	0.010	0.348
Dimethoate	AEM 4	0.943	-0.289	0.014	0.291
Dimethoate	AEM 5	0.983	-0.963	0.003	0.964
Atrazine	AEM 1	0.886	-0.098	0.109	0.098
Atrazine	AEM 2	0.930	-0.272	0.012	0.273
Atrazine	AEM 3	0.931	-0.374	0.017	0.375
Atrazine	AEM 4	0.989	-0.337	0.037	0.338
Atrazine	AEM 5	0.966	-0.364	0.030	0.365
Simazine	AEM 1	0.868	-0.101	0.092	0.101
Simazine	AEM 2	0.900	-0.139	0.034	0.140
Simazine	AEM 3	0.964	-0.266	0.013	0.266
Simazine	AEM 4	0.976	-0.297	0.035	0.298
Simazine	AEM 5	0.973	-0.307	0.039	0.308
Caffeine	AEM 1	0.748	-0.067	0.027	0.067
Caffeine	AEM 2	0.954	-0.279	0.005	0.279
Caffeine	AEM 3	0.959	-0.167	0.007	0.167
Caffeine	AEM 4	0.961	-0.220	0.006	0.220
Caffeine	AEM 5	0.935	-0.120	0.017	0.121
Paracetamol	AEM 1	0.743	-0.074	0.088	0.074
Paracetamol	AEM 2	0.981	-0.207	0.017	0.207
Paracetamol	AEM 3	0.934	-0.197	0.029	0.198
Paracetamol	AEM 4	0.957	-0.199	0.018	0.200
Paracetamol	AEM 5	0.972	-0.326	0.009	0.327

Table S3. Normalized adsorption function parameters and their coefficients of determination for cation exchange membranes. Related to Figure 3.

		R^2	a	b	c
Diuron	CEM 1	0.943	-0.406	0.015	0.406
Diuron	CEM 2	0.971	-0.499	0.014	0.499
Diuron	CEM 3	0.978	-0.592	0.028	0.594
Diuron	CEM 4	0.975	-0.730	0.011	0.733
Diuron	CEM 5	0.965	-0.762	0.014	0.763
Dimethoate	CEM 1	0.886	-0.105	0.051	0.105
Dimethoate	CEM 2	0.977	-0.169	0.013	0.169
Dimethoate	CEM 3	0.989	-0.388	0.003	0.388
Dimethoate	CEM 4	0.970	-0.237	0.014	0.238
Dimethoate	CEM 5	0.968	-0.714	0.003	0.714
Atrazine	CEM 1	0.828	-0.212	0.018	0.210
Atrazine	CEM 2	0.983	-0.359	0.024	0.358
Atrazine	CEM 3	0.997	-0.590	0.025	0.590
Atrazine	CEM 4	0.999	-0.601	0.024	0.601
Simazine	CEM 1	0.858	-0.121	0.064	0.120
Simazine	CEM 2	0.974	-0.365	0.028	0.364
Simazine	CEM 3	0.995	-0.550	0.033	0.551
Simazine	CEM 4	1.000	-0.590	0.029	0.590
Caffeine	CEM 1	0.938	-0.066	0.391	0.066
Caffeine	CEM 2	0.969	-0.152	0.135	0.152
Caffeine	CEM 3	0.921	-0.100	0.132	0.100
Caffeine	CEM 4	0.384	-0.057	0.510	0.057
Caffeine	CEM 5	0.986	-0.243	0.062	0.243
Paracetamol	CEM 1	0.964	-0.065	0.143	0.065
Paracetamol	CEM 2	0.994	-0.114	0.024	0.114
Paracetamol	CEM 3	0.886	-0.174	0.036	0.174
Paracetamol	CEM 4	0.949	-0.135	0.032	0.135
Paracetamol	CEM 5	0.919	-0.141	0.030	0.141

Table S4. Normalized transport function parameters and their coefficients of determination for anion exchange membranes. Related to Figure 3.

		R^2	a	b	c
Diuron	AEM 1	0.877	-0.345	0.026	0.303
Diuron	AEM 2	0.890	-0.446	0.055	0.139
Diuron	AEM 3	0.853	-1.089	0.002	1.000
Diuron	AEM 4	0.413	-0.126	0.036	0.038
Diuron	AEM 5	0.130	-19.077	0.248	0.010
Dimethoate	AEM 1	0.863	-0.189	0.016	0.183
Dimethoate	AEM 2	0.816	-0.181	0.007	0.145
Dimethoate	AEM 3	0.903	-0.556	0.002	0.514
Dimethoate	AEM 4	0.617	-45.498	0.170	0.031
Dimethoate	AEM 5	0.904	-0.155	0.007	0.121
Atrazine	AEM 1	0.621	-0.117	0.024	0.099
Atrazine	AEM 2	0.848	-55.161	0.123	0.012
Atrazine	AEM 3	0.793	-0.110	0.006	0.068
Atrazine	AEM 4	0.362	-48.246	0.155	0.001
Atrazine	AEM 5	0.147	-0.020	0.013	0.016
Simazine	AEM 1	0.853	-0.239	0.013	0.229
Simazine	AEM 2	0.852	-0.286	0.005	0.229
Simazine	AEM 3	0.756	-0.809	0.001	0.759
Simazine	AEM 4	0.921	-0.180	0.004	0.151
Simazine	AEM 5	0.217	-39.545	0.179	0.021
Caffeine	AEM 1	0.925	-0.057	0.009	0.059
Caffeine	AEM 2	0.830	-0.048	0.003	0.048
Caffeine	AEM 3	0.814	-0.143	0.001	0.141
Caffeine	AEM 4	0.073	-34.343	0.180	0.015
Caffeine	AEM 5	0.803	-47.310	0.119	0.021
Paracetamol	AEM 1	0.933	-0.423	0.029	0.416
Paracetamol	AEM 2	0.943	-1.013	0.003	1.000
Paracetamol	AEM 3	0.895	-1.025	0.002	1.000
Paracetamol	AEM 4	0.941	-1.012	0.003	1.000
Paracetamol	AEM 5	0.830	-1.060	0.002	1.000

Table S5. Normalized transport function parameters and their coefficients of determination for cation exchange membranes. Related to Figure 3.

		R^2	a	b	c
Diuron	CEM 1	0.939	-1.010	0.003	0.950
Diuron	CEM 2	0.822	-0.481	0.005	0.382
Diuron	CEM 3	0.845	-49.683	0.111	0.023
Diuron	CEM 4	0.143	0.000	0.139	0.000
Diuron	CEM 5	0.001	0.000	0.568	0.000
Dimethoate	CEM 1	0.836	-1.023	0.001	0.986
Dimethoate	CEM 2	0.924	-0.506	0.002	0.465
Dimethoate	CEM 3	0.854	-0.669	0.001	0.660
Dimethoate	CEM 4	0.053	-0.053	0.518	0.003
Dimethoate	CEM 5	0.172	-26.498	0.360	0.014
Atrazine	CEM 1	0.582	-42.056	0.153	0.028
Atrazine	CEM 2		-46.536	0.214	0.001
Atrazine	CEM 3	0.092	0.000	0.657	0.000
Atrazine	CEM 4	0.208	0.000	0.033	0.000
Simazine	CEM 1	0.883	-0.658	0.005	0.600
Simazine	CEM 2	0.608	-37.469	0.143	0.035
Simazine	CEM 3	0.282	0.000	0.557	0.000
Simazine	CEM 4	0.438	0.000	0.511	0.000
Caffeine	CEM 1	0.995	-0.494	0.037	0.477
Caffeine	CEM 2	0.999	-0.463	0.029	0.435
Caffeine	CEM 3	0.751	-1.052	0.005	1.000
Caffeine	CEM 4	0.983	-0.409	0.020	0.454
Caffeine	CEM 5	0.910	-0.704	0.008	0.635
Paracetamol	CEM 1	0.810	-1.053	0.003	1.000
Paracetamol	CEM 2	0.750	-0.507	0.008	0.445
Paracetamol	CEM 3	0.543	-0.632	0.002	0.590
Paracetamol	CEM 4	0.873	-0.542	0.002	0.503
Paracetamol	CEM 5	0.837	-1.039	0.001	0.993

Contact angle measurements

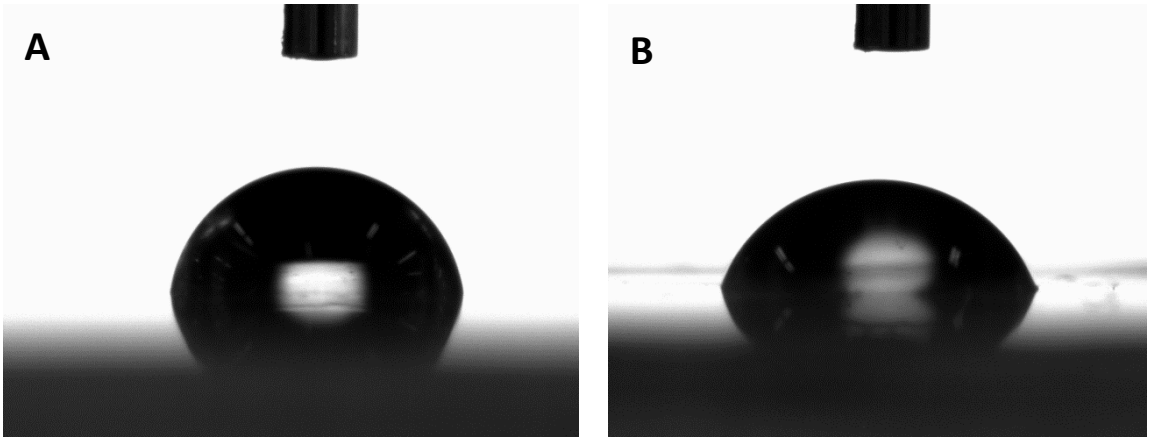

Figure S3. Example of contact angle measurement for (A) anion-exchange membranes (AEM1dry = 15.4 ± 0.2 [µm]) and (B) cation-exchange membranes (CEM1dry = 17.7 ± 0.6 [µm]). Related to Figure 4 and discussed in the manuscript's 2.3.1 section.

Table S6. Values of contact angle measured on anion-exchange (AEM1dry = 15.4 ± 0.2 [µm]) and cation-exchange membranes (CEM1dry = 17.7 ± 0.6 [µm]). Related to Figure 4 and discussed in the manuscript's 2.3.1 section.

AEM contact angle [°]	AEM Droplet volume [µL]	CEM contact angle [°]	CEM Droplet volume [µL]
84.095	2.127	68.290	2.087
76.655	1.785	73.900	1.629
82.541	1.672	70.050	1.539
78.443	1.525	71.224	1.661
80.631	1.893	67.517	1.544
79.293	1.834	74.194	1.673
85.507	2.061	71.520	1.618

Diffusion and adsorption coefficients determined by non-steady diffusion-adsorption model

Table S7. Diffusion coefficients with standard errors in anion-exchange membranes. Related to Figure 5.

AEM thickness [µm]	D_{Diuron} [m^2 s^{-1}]	Standard error	$D_{Dimethoate}$ [m^2 s^{-1}]	Standard error	$D_{Atrazine}$ [m^2 s^{-1}]	Standard error	$D_{Simazine}$ [m^2 s^{-1}]	Standard error	$D_{Caffeine}$ [m^2 s^{-1}]	Standard error	$D_{Paracetamol}$ [m^2 s^{-1}]	Standard error
15.9	1.02E-11	2.97E-12	3.41E-12	1.55E-12	2.03E-12	7.21E-13	3.18E-12	1.03E-12	8.70E-13	1.88E-13	7.76E-12	2.42E-12
33.4	1.26E-11	2.11E-12	4.57E-12	1.69E-12	1.93E-12	4.11E-13	3.31E-12	5.74E-13	1.53E-12	5.36E-13	8.59E-12	2.82E-12
42.3	1.21E-11	1.27E-12	3.72E-12	5.75E-13	2.33E-12	4.03E-13	3.85E-12	5.83E-13	1.44E-12	3.49E-13	1.11E-11	8.52E-13
71	2.18E-11	2.59E-12	7.64E-12	1.83E-12	4.61E-12	6.62E-13	6.80E-12	7.42E-13	2.74E-12	4.85E-13	2.08E-11	2.33E-12
89.6	3.00E-11	4.86E-12	8.81E-12	1.03E-12	8.41E-12	2.38E-12	1.11E-11	3.71E-12	4.57E-12	1.45E-12	2.08E-11	2.91E-12

Table S8. Adsorption coefficients with standard errors in anion-exchange membranes. Related to Figure 5.

AEM thickness [µm]	k_{Diuron} [s^{-1}]	Standard error	$k_{Dimethoate}$ [s^{-1}]	Standard error	$k_{Atrazine}$ [s^{-1}]	Standard error	$k_{Simazine}$ [s^{-1}]	Standard error	$k_{Caffeine}$ [s^{-1}]	Standard error	$k_{Paracetamol}$ [s^{-1}]	Standard error
15.9	5.10E-02	7.41E-03	1.68E-02	7.27E-03	2.35E-02	1.97E-03	2.34E-02	2.37E-03	1.17E-02	6.66E-03	5.55E-03	4.83E-03
33.4	4.64E-02	2.43E-03	1.02E-02	1.17E-03	1.22E-02	1.37E-03	8.31E-03	4.83E-04	9.26E-03	3.66E-03	1.19E-02	3.17E-03
42.3	5.01E-02	7.22E-03	1.07E-02	2.91E-03	1.74E-02	3.92E-03	1.23E-02	2.91E-03	6.10E-03	2.32E-03	8.52E-03	8.86E-04
71	3.91E-02	3.21E-03	7.57E-03	1.05E-03	1.33E-02	1.93E-03	8.99E-03	1.98E-03	2.99E-03	5.52E-04	3.05E-03	1.42E-03
89.6	4.78E-02	2.10E-03	7.99E-03	1.61E-03	1.14E-02	5.39E-03	7.64E-03	3.13E-03	2.53E-03	4.14E-04	3.05E-03	1.99E-03

Table S9. Diffusion coefficients with standard errors in cation-exchange membranes. Related to Figure 5.

CEM thickness [µm]	D_{Diuron} [m^2 s^{-1}]	Standard error	$D_{Dimethoate}$ [m^2 s^{-1}]	Standard error	$D_{Caffeine}$ [m^2 s^{-1}]	Standard error	$D_{Paracetamol}$ [m^2 s^{-1}]	Standard error
19	6.12E-12	3.77E-12	2.48E-12	6.18E-13	2.42E-11	2.90E-11	5.51E-12	2.18E-12
36.3	8.36E-12	2.19E-12	3.90E-12	2.73E-13	5.35E-12	1.72E-12	7.85E-12	1.98E-12
51.3	9.56E-12	2.56E-12	3.96E-12	1.28E-12	1.04E-11	7.54E-12	8.38E-12	2.56E-12
76.7	9.76E-12	3.25E-12	4.25E-12	9.14E-13	4.62E-12	6.84E-13	8.05E-12	2.26E-12
84.4	1.24E-11	1.60E-12	4.66E-12	5.50E-13	2.40E-11	1.69E-11	8.24E-12	8.33E-13

Table S10. Adsorption coefficients with standard errors in cation-exchange membranes. Related to Figure 5.

CEM thickness [µm]	kDiuron [s^{-1}]	Standard error	kDimethoate [s^{-1}]	Standard error	kCaffeine [s^{-1}]	Standard error	kParacetamol [s^{-1}]	Standard error
19	2.80E-02	7.70E-03	1.51E-02	8.61E-03	1.01E-02	1.12E-02	1.14E-02	6.22E-03
36.3	2.47E-02	2.14E-03	1.23E-02	7.79E-03	1.95E-02	7.70E-03	8.37E-03	4.72E-03
51.3	2.86E-02	3.59E-03	6.74E-03	2.57E-03	5.60E-03	2.21E-03	9.50E-03	4.12E-03
76.7	2.41E-02	3.99E-03	7.58E-03	2.53E-03	1.93E-03	1.93E-03	3.77E-03	6.17E-04
84.4	2.46E-02	3.79E-03	6.66E-03	2.35E-03	4.13E-03	5.48E-04	6.90E-03	3.28E-03

pH measurements in performed experiments

Table S11. pH measured during experiments containing anion exchange membranes. Related to Figure 5 and discussed in the manuscript's 2.3.2 section.

AEM 1	**Exp 1**	**Time [h]**	0	6	24	48	72	117	
		pH Feed	5.61	5.67	5.75	5.79	5.98	5.63	
		pH Permeate	6.24	5.82	5.72	5.76	5.69	5.48	
	Exp 2	**Time [h]**	0	12	24	48	52	55.5	
		pH Feed	5.78	5.35	5.57	5.66	5.54	5.87	
		pH Permeate	5.34	5.49	5.49	5.35	5.36	5.64	
AEM 2	**Exp 1**	**Time [h]**	0	8	24	48	72	93	
		pH Feed	5.64	5.57	5.53	5.59	5.65	5.11	
		pH Permeate	5.89	5.52	5.48	5.66	5.7	5.06	
	Exp 2	**Time [h]**	0	10	24	48	50	55.5	
		pH Feed	5.59	6.61	5.34	5	4.79	5.1	
		pH Permeate	5.66	5.76	5.67	5.31	5.28	5.39	
AEM 3	**Exp 1**	**Time [h]**	0	21	93	117			
		pH Feed	5.9	5.24	4.9	4.92			
		pH Permeate	5.81	5	4.98	4.84			
	Exp 2	**Time [h]**	0	8	25	30	56	79	
		pH Feed	5.57	5.4	5.34	5.57	5.63	5.6	
		pH Permeate	5.62	6.67	5.44	5.52	5.76	5.73	
AEM 4	**Exp 1**	**Time [h]**	0	8	25	30	56	79	
		pH Feed	5.63	5.94	5.68	5.76	5.84	5.7	
		pH Permeate	5.84	5.87	5.72	5.81	5.78	5.83	
	Exp 2	**Time [h]**	0	4	21	45	69	93	117
		pH Feed	5.38	4.47	5.54	5.6	5.62	5.55	5.62
		pH Permeate	5.48	5.53	5.55	5.67	5.6	5.48	5.5
AEM 5	**Exp 1**	**Time [h]**	0	21	45	69	93	117	
		pH Feed	5.78	5.72	5.69	5.72	5.64	5.79	
		pH Permeate	5.74	5.75	5.78	5.75	5.8	5.73	
	Exp 2	**Time [h]**	0	6	9	24	56	79	
		pH Feed	5.9	5.92	5.94	5.88	5.95	5.96	
		pH Permeate	5.84	5.88	5.9	5.9	5.87	5.88	

Table S12. pH measured during experiments containing cation exchange membranes. Related to Figure 5 and discussed in the manuscript's 2.3.2 section.

CEM 1	**Exp 1**	**Time [h]**	0	6	24	48	72	120	
		pH Feed	6	6.05	5.93	5.94	5.95	6.3	
		pH Permeate	6.3	6.01	6.08	6.05	5.93	5.95	
	Exp 2	**Time [h]**	0	12	24	48	52	55.5	
		pH Feed	4.82	3.78	3.74	3.72	3.75	3.73	
		pH Permeate	4.75	3.89	3.88	3.85	3.8	3.81	
CEM 2	**Exp 1**	**Time [h]**	0	6	24	48	72	120	
		pH Feed	5.92	6.08	6.09	6.05	5.94	6.1	
		pH Permeate	6.15	6.12	6.15	6.08	5.77	5.75	
	Exp 2	**Time [h]**	0	10	24	48	50	55.5	
		pH Feed	4.85	3.72	3.69	3.72	3.73	3.85	3.74
		pH Permeate	4.35	3.68	3.73	3.75	3.81	3.8	3.77
CEM 3	**Exp 1**	**Time [h]**	0	21	93	117			
		pH Feed	5.9	5.24	4.9	3.76			
		pH Permeate	5.81	5	4.76	3.8			
	Exp 2	**Time [h]**	0	8	25	30	56	79	
		pH Feed	4.63	4.29	3.92	3.78	3.52	3.49	
		pH Permeate	4.98	4.13	4	3.82	3.65	3.14	
CEM 4	**Exp 1**	**Time [h]**	0	4	21	45	69	93	117
		pH Feed	6	6.02	6.1	6.15	6.21	6.19	6.26
		pH Permeate	6.58	6.49	6.37	6.44	6.46	6.47	6.41
	Exp 2	**Time [h]**	0	4	21	45	69	93	117
		pH Feed	4.37	4.23	3.88	3.78	3.52	3.41	3.47
		pH Permeate	4.29	4.13	3.76	3.82	3.65	3.55	3.61
CEM 5	**Exp 1**	**Time [h]**	0	21	45	69	93	117	
		pH Feed	5.98	5.99	5.88	5.91	5.99	5.99	
		pH Permeate	6.04	6.11	6.19	6.15	6.13	6.11	
	Exp 2	**Time [h]**	0	6	9	24	56	79	
		pH Feed	4.51	4.23	3.4	3.61	3.55	3.61	
		pH Permeate	4.82	4.59	4.05	3.67	3.59	3.55	

Regression parameters of exponential fit between diffusion coefficient and membrane thickness.

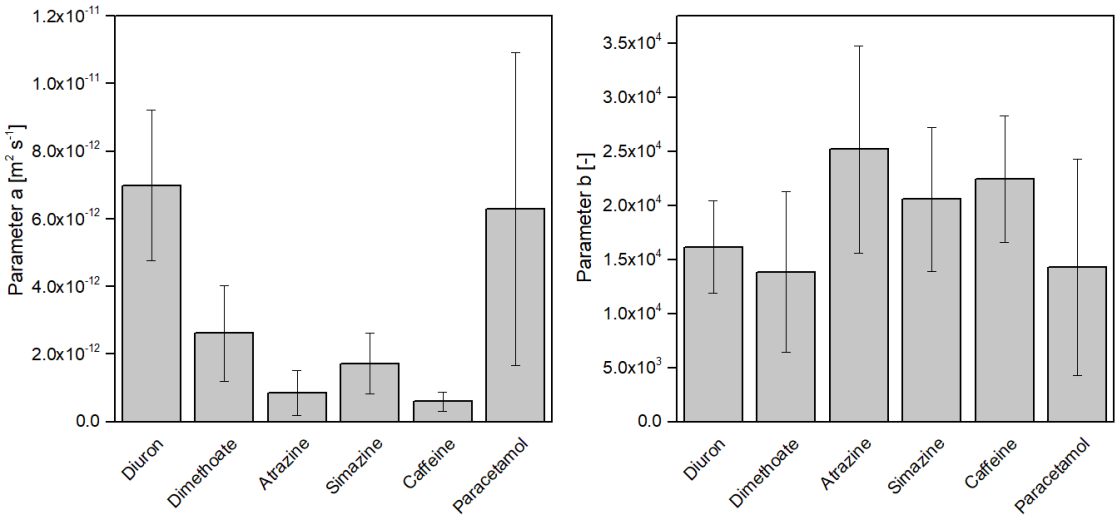

Figure S4. Regression parameters of exponential fit between diffusion coefficient and membrane thickness in anion-exchange membranes. Related to Figure 5 and discussed in the manuscript's 2.3.2 section.

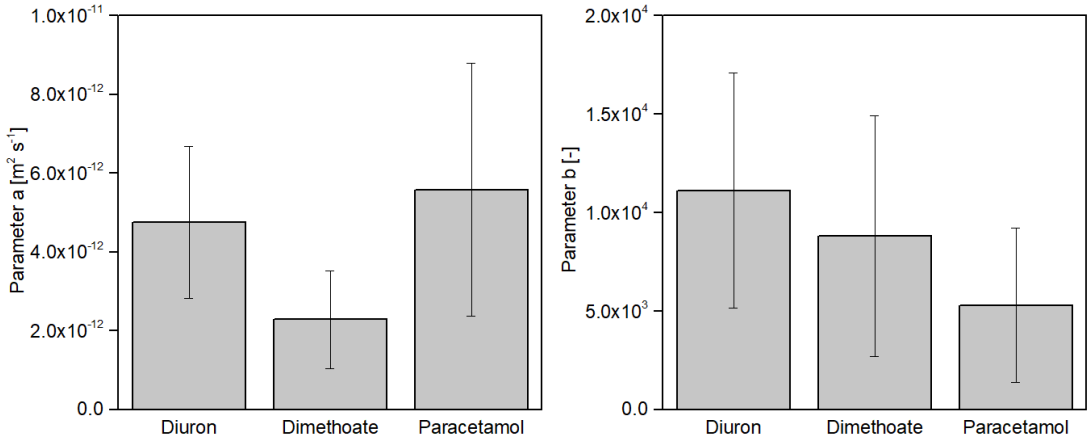

Figure S5. Regression parameters of exponential fit between diffusion coefficient and membrane thickness in cation-exchange membranes. Related to Figure 5 and discussed in the manuscript's 2.3.2 section.

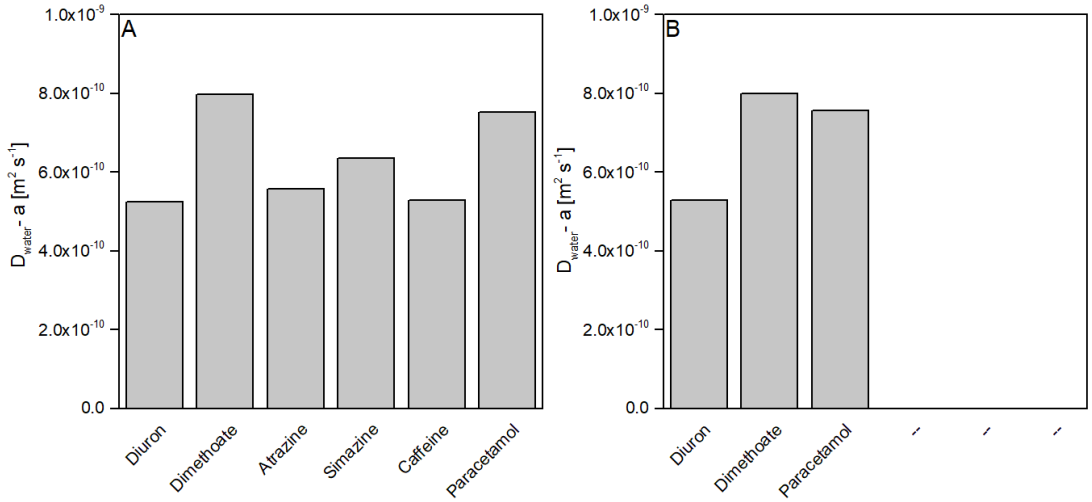

Figure S6. Difference between regression parameter a and diffusion coefficients of OMPs in water in AEMs (A) and CEMs (B). The diffusion coefficients for diuron, dimethoate, atrazine, simazine, caffeine, and paracetamol were found in (GSI Environmental, 2020c, GSI Environmental, 2020b, GSI Environmental, 2020a, GSI Environmental, 2020d, Bichsel, 1979, Ma et al., 2018), respectively. Related to Figure 5 and discussed in the manuscript's 2.3.2 section.

Transparent Methods

Organic micropollutants used in experiments

Table S13. Physio-chemical properties of organic micropollutants (https://chemicalize.com, 2019). Related to Figure 1-5.

Compound	LogP	LogD (6.5 pH)	M	Formal charge (6.5 pH)	Molar refractiviy	Polarizability	Atom count	Heavy atom count	Asymmetric atom count	Rotatable bond count	Ring count	Aromatic ring count	Hetero ring count	Hydrogen donor/acceptor count	Van der Waals volume	Van der Waals surface	Topological polar surface area	Solvent accessible surface area	Min projection area	Max projection area	Min projection radius	Max projection radius
	[-]	[-]	[g/mol]	[-]	[cm^3/mol]	[$Å^3$]	[-]	[-]	[-]	[-]	[-]	[-]	[-]	[-]	[$Å^3$]	[$Å^2$]	[$Å^2$]	[$Å^2$]	[$Å^2$]	[$Å^2$]	[Å]	[Å]
lincomycin	0.2	-1.8	406.5	0.97	102.67	41.49	66	29	9	7	2	0	2	12	384.93	625.68	122.49	627.54	64.29	105.56	5.34	8.31
metoprolol	1.76	-1.14	267.4	1	76.76	30.34	44	19	1	9	1	1	0	6	274.25	474.8	50.72	602.12	37.99	93.27	4.39	10.07
atenolol	0.43	-2.48	266.3	1	73.51	29.09	41	19	1	8	1	1	0	7	261.34	440.22	84.58	534.33	36.85	87.58	4.19	9.12
propanolol	2.58	-0.32	259.3	1	76.83	31.77	40	19	1	6	2	2	0	5	257.56	427.55	41.49	504.57	41.97	85.55	4.66	7.41
pirimicarb	1.8	1.78	238.3	0.24	66.65	24.34	35	17	0	3	1	1	1	4	227.99	398.25	58.56	542	44.01	73.22	4.99	6.49
salbutamol	0.34	-2.01	239.3	1	67.87	26.58	38	17	1	5	1	1	0	8	239.15	406.23	72.72	463.93	41.28	74.32	4.32	6.96
terbutaline	0.44	-1.45	225.3	0.99	63.04	24.73	35	16	1	4	1	1	0	8	222.28	375.48	72.72	436.62	39.07	69.95	4.18	6.47
diclofenac	4.26	1.79	296.2	-1	75.46	29.03	30	19	0	4	2	2	0	5	236.85	360.28	49.33	424.95	40.96	78.63	4.62	6.34
triclopyr	2.7	-0.75	256.5	-1	52.24	20.43	18	14	0	3	1	1	1	5	173.35	262.07	59.42	391.34	30.91	65.22	4.15	6.19
ketoprofen	3.61	1.05	254.3	-1	72.52	28.01	33	19	1	4	2	2	0	4	233.68	367.5	54.37	452.27	41.68	72.81	4.37	6.58
fenoprofen	3.65	1.15	243.3	-1	68.18	26.68	32	18	1	4	2	2	0	3	223.44	356.95	46.53	446.28	40.56	71.3	4.28	6.49
clof acid	2.9	-0.08	214.7	-1	52.62	20.8	25	14	0	3	1	1	0	4	184.05	302	46.53	372.83	30.34	58.91	3.5	6.2
ibuprofen	3.84	2.19	206.3	-0.98	60.73	23.65	33	15	1	4	1	1	0	3	211.8	356.4	37.3	430.24	35.44	64.57	3.78	6.59
diuron	2.53	2.53	233.1	0	59	22.02	24	14	0	1	1	1	0	2	187.06	295.9	32.34	402.13	28.58	69.92	3.93	6.5
dimethoate	0.34	0.34	229.3	0	55.34	22.38	24	12	0	5	0	0	0	2	184.48	308.11	47.56	439.77	35.75	61.36	4.09	6.04
atrazine	2.2	2.2	215.7	0	62.22	21.19	28	14	0	4	1	1	1	7	190.9	324.67	62.73	471.23	39.04	66.08	4.79	6.36
simazine	1.78	1.78	201.7	0	57.8	19.37	25	13	0	4	1	1	1	7	173.73	294.95	62.73	454.65	35.92	65	5.14	6.4
caffeine	-0.55	-0.55	194.2	0	49.83	17.87	24	14	0	0	2	2	2	3	164.25	269.12	58.44	368.37	30.68	62.2	4.34	5.03
paracetamol	0.91	0.91	151.2	0	42.9	15.82	20	11	0	1	1	1	0	4	138.08	222.91	49.33	331.99	21.65	54.37	3.49	5.67

Organic micropollutants and chemical analysis

A 2 mg L^{-1} stock solution of nineteen OMPs (analytical grade, Sigma-Aldrich, >98%) was prepared and stored at 4 °C. A complete list of used OMPs with their chemical formula and physicochemical properties is included in Table S13 and S14. The primary reasoning behind the OMPs' selection was to work with relatively large group, representing known chemicals of different usage, such as pharmaceuticals (e.g., paracetamol), beverages (e.g., caffeine), and herbicides (e.g., diuron). Furthermore, as the group should vary in charge, 6 positively-, 7 negatively- and 6 non-charged OMPs were selected. Besides charge, selected OMPs were characterized by a variety of other physicochemical parameters, i.e., hydrophobicity, size, presence of specific groups.

The concentration of OMPs in solution was analyzed by a liquid chromatography-mass spectrometry (Agilent 6420 LC-MS/MS) with a selective electrospray triple quad LC-MS/MS MRM transition. A Phenomenex phenyl-hexyl column (150 mm×3 mm, 3 µm pore size) equipped with a guard column was used for chromatography separation. The aqueous neutral mobile phase was prepared with 2.5 L Milli-Q water, 5 mL ammonia 5 M, 1 mL formic acid (99%), and 0.1 mL oxalic acid (1M). Acetonitrile was used as an organic mobile phase. The samples (1 mL) were spiked with a matrix modifier (50 µL) and an internal standard (50 µL) prior to analysis. For data analysis, the Agilent Mass Hunter Quant software was used to integrate and quantitate the peaks in the data files.

Selection of Ion Exchange Membranes

To mimic the average IEMs system, experiments were performed on tailored AEMs and CEMs designed for ED and RED processes. Fumasep FAS (anion-exchange) and FKS (cation-exchange) membranes (FumaTech GmbH, Germany) were selected as homogenous membranes. Standard grade Fumasep FAS and FKS membranes data, given by Fumatech can be found in Table S15.

Table S14. Properties of standard grade Fumasep FAS and FKS membranes. Related to Figure 1-5 and Table S1.

	Type	**Reinforcement**	**Thickness µm**	**IEC meq g^{-1}**	**Selectivity %**	**Specific area resistance Ω cm^2**	**Stability pH**
FAS	anion	none	10 - 50	1.6 - 1.8	94 - 97	0.4 - 0.8	1 - 14
FKS	cation	none	10 - 50	1.3 - 1.4	98 - 99	0.9 - 1.9	1 - 14

For this study, membrane thickness was a key control parameter. On a special request, membranes were prepared in five different thicknesses of each type (AEMs and CEMs), further denoted as an AEM1, AEM2, AEM3, AEM4, AEM5, and CEM1, CEM2, CEM3, CEM4, CEM5. Thicknesses varied between 15 and 85 µm and increased in the following order: AEM1/CEM1 < AEM2/CEM2 < AEM3/CEM3 < AEM4/CEM4 < AEM5/CEM5. Wet and dry membrane thicknesses were measured using optical microscopy. Measurements were conducted thirty times for each thickness of both AEMs and CEMs at different membrane locations. The swelling degree of the membranes was calculated according to (1):

$$swelling\ degree = \frac{x_{wet} - x_{dry}}{x_{dry}} \cdot 100\% \qquad \textbf{(1)}$$

Where, x_{wet} and x_{dry} are wet and dry membrane thicknesses, respectively [µm].

Each type of membranes was prepared with the same polymer solution (i.e., the same polymer batch); thus, providing the same chemical properties to each membrane sheet. AEMs and CEMs were received in a dry form. Prior to the experiments, membranes were pretreated according to the manufacturer instructions, i.e., soaked in MilliQ water for 48h to remove any preservatives, whereby MilliQ was refreshed after the first 24h. Additionally, CEMs were protonated for one hour in a 0.1 M H_2SO_4 solution.

Characterization of the membrane polymer structure using PALS

Positron annihilation lifetime spectroscopy allows the measurement of FVEs inside polymeric membranes and was used in this work to characterize the size and abundance of FVEs inside dry IEMs. Positron annihilation lifetime spectroscopy (PALS) is based on the interaction of positrons (e^+), the antiparticle of electrons (e^-), with the matter. Upon implantation of a e^+ in material here, the ion-exchange membranes (IEM), the e^+ will undergo different deceleration processes, mainly the scattering with optical phonons, until reaching thermal equilibrium. Subsequent diffusion through the material leads to the annihilation with an e^- from the material. In polymers, the e^+ can also be trapped inside the free volume element (FVE) located between polymer chains and can then form an e^+e^- bound state the so-called positronium (Ps). Ps exist as *para*-Ps (p-Ps) and *ortho*-Ps (*o*-Ps), in singlet and triplet state, respectively. Especially the *o*-Ps lifetime is interesting in polymer samples, as the e^+ of the *o*-Ps can annihilate with an e^- from the FVE wall and, therefore, reduce the vacuum lifetime of *o*-Ps (142 ns) considerably. This process is called 'pick-off annihilation' and the corresponding lifetime (i.e. the e^+ lifetime between implantation and pick-off annihilation) is material dependent and can be related to the size of the FVE by the Tao-Eldrup model (2) (Tao, 1972, Eldrup et al., 1981).

$$\tau_{pick-off} = \frac{1}{2} * \left[1 - \frac{r}{r+\Delta r} + \frac{1}{2\pi}\sin\left(\frac{2\pi r}{r+\Delta r}\right)\right]^{-1} [ns] \qquad \textbf{(2)}$$

With Δr, an empirically found value describing the overlap of o-Ps wave function and the material around the FVE. (set at 0.166 nm (Eldrup et al., 1981)).The longer the pick-off lifetime, the bigger the FVE, and vice versa. Additionally, the intensity of the *o*-Ps lifetime component can be used, in some cases, to estimate relative changes in free volume abundance.

The PALS lifetime spectra were measured with the pulsed low energy positron beam system (PLEPS) operated at the neutron-induced positron source Munich (NEPOMUC) located at the FRM-II reactor in Germany (Hugenschmidt et al., 2008, Hugenschmidt et al., 2012, Egger et al., 2007, Sperr et al., 2008). PALS measurements with implantation energies varying between 1 and 18 keV were executed under UHV conditions. Implantation depths were calculated, as described elsewhere (Algers et al., 2003), based on a polymer sample density of 1.2 g/cm³ and 0.96 g/cm³ for AEMs and CEMs, respectively, calculated as the ratio between mass and volume of 5×5 cm² membrane piece. For every spectrum, 4 million counts were collected at a count rate of ca. 10 000 counts/s with an overall time resolution of ca. 250 ps. The instrument resolution function was determined by measuring p-doped SiC, a sample with known lifetimes. All spectra were evaluated with PALSfit*3* software (Kirkegaard et al., 2017) and split into four-lifetime components corresponding to *para*-positronium (*p*-Ps), the annihilation of free e^+, and the pick-off annihilation of *ortho*-positronium (*o*-Ps) (one or two lifetime components). The reduced chi-square values were below 1.2 for all fits. The longest *o*-Ps lifetime component showed a significantly low intensity in all samples and was considered as an artefact of data analysis and surface effects. It was therefore not considered as a material property and is hence not taken into consideration in the discussion.

OMP diffusion experiments

Two-compartment glass cells with a maximum capacity of 250 mL were used for diffusion experiments, as described in (Ma et al., 2018). The feed solution contained a mixture of OMPs (50 μgL^{-1} for each organic solute), while the permeate solution (i.e., the compartment initially not containing OMPs) contained only Milli-Q water. The compartments were separated by a selected IEM of 5.94 cm^2 surface area. Both compartments were continuously stirred at 500 rpm. The experiment was performed at a temperature of 23 ± 3°C for up to 120 hours. This time range was selected arbitrarily as sufficient time to observe the diffusion of OMPs toward permeate in low concentration difference regime. 1 mL of sample was collected at different time intervals in both compartments. Each sample was collected and measured in triplicate. To determine the adsorption and transport over the experimental time at different time intervals, the mass balances were calculated for all OMPs individually according (3) and (4):

$$transport = \left(\frac{n_P(t)}{n_F(0)} \cdot 100\%\right) \qquad \textbf{(3)}$$

$$adsorption = \left(1 - \left(\frac{n_F(t)+n_P(t)}{n_F(0)}\right)\right) \cdot 100\% \qquad \textbf{(4)}$$

Where, $n_F(0)$ is the initial amount of OMP [mol] in feed, which is the total amount of OMP in the system. $n_F(t)$ and $n_P(t)$ are the amounts of OMP [mol] in feed and permeate, respectively, at a specific time of the experiment.

OMPs natural degradation and glass adsorption control experiment

A 250 mL glass vessel containing 200 mL experimental solution of OMPs was located on a stirring plate for 96h. Each measurement was performed in a triplicate. Concentrations of OMPs measured during the control experiment remained constant.

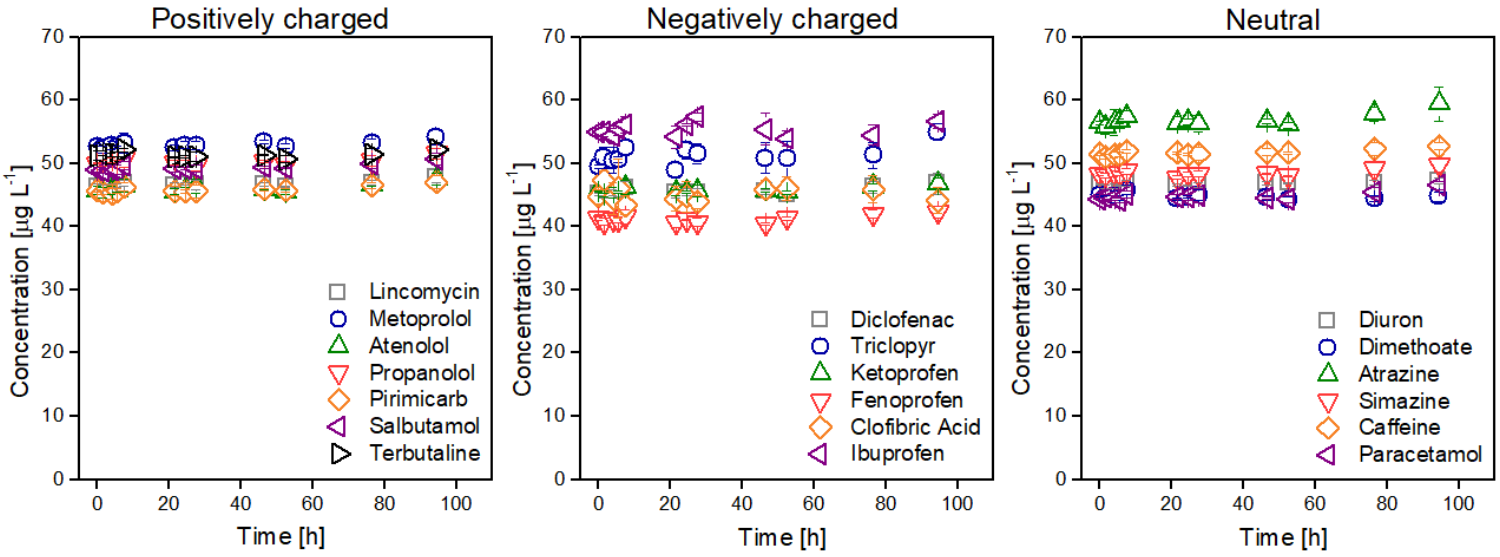

Figure S7. Concentrations of OMPs measured during the control experiment. Related to Figure 2, Figure S1 and S2, and discussed in the manuscript's 2.2. and 2.3.1. section.

Dynamic diffusion-adsorption model for determination of transport coefficients of organic micropollutants in IEM

The diffusion process through the membrane was modeled based on diffusion physics by using a partial differential equation (PDE) derived from Fick's second law for non-steady state diffusion as follows:

$$\frac{\partial n(x,t)}{\partial t} = D\,\frac{\partial^2 n(x,t)}{\partial x^2} - k \cdot n(x,t) \qquad \textbf{(5)}$$

With a Dirichlet boundary condition at x = 0: $n(0,t) = n_F(t)$, where $n_F(t)$ is found from the mass balance of the feed, and a Neumann boundary condition $D\,\frac{\partial n(x,t)}{\partial x} = 0$ at x = x_{wet}, where x_{wet} is the wet membrane thickness. This equation was used to calculate the solution $n(x,t)$. In Equation S14.1, $n(x,t)$ indicates the distribution of a certain OMP in the membrane profile, whereas k is the adsorption, and D the diffusion coefficient. Equation S14.1 was solved for the wet thickness of each membrane by the Matlab PDE tool, where both boundary conditions were treated as internal boundary conditions.

The nonlinear least-squares (NLS) method was used to estimate the diffusion (D) and adsorption (k) coefficient, where the standard deviation of estimates is calculated from the covariance matrix (based on parameter sensitivities, number of measuring points, and residual error between measuring points and the model output).

To identify the smallest residual error, parameters D and k were changed in an iterative procedure, induced by the NLS method. During each iteration, a general partial differential equation (PDE; parabolic equation $d\frac{\partial u}{\partial t} - \nabla \cdot (c\nabla u) + au = f$, with d=1, c:=D, a:=k and f=0) was solved using finite element analysis for a geometry corresponding to the experimental setup (i.e., for each node of the mesh at each time instance). No flux through the boundary (Neumann) conditions were applied for the outer

boundaries of the geometry, and internal Dirichlet and Neumann boundary conditions were applied between membrane and solution. For the time-domain, a duration of 120 hours was used with time steps of 30 min.
Below are the model outcomes (concentration in nodes) for the same experimental data but at different time, that is after 5 (Figure S8.) and after 115 hours (Figure S9.).

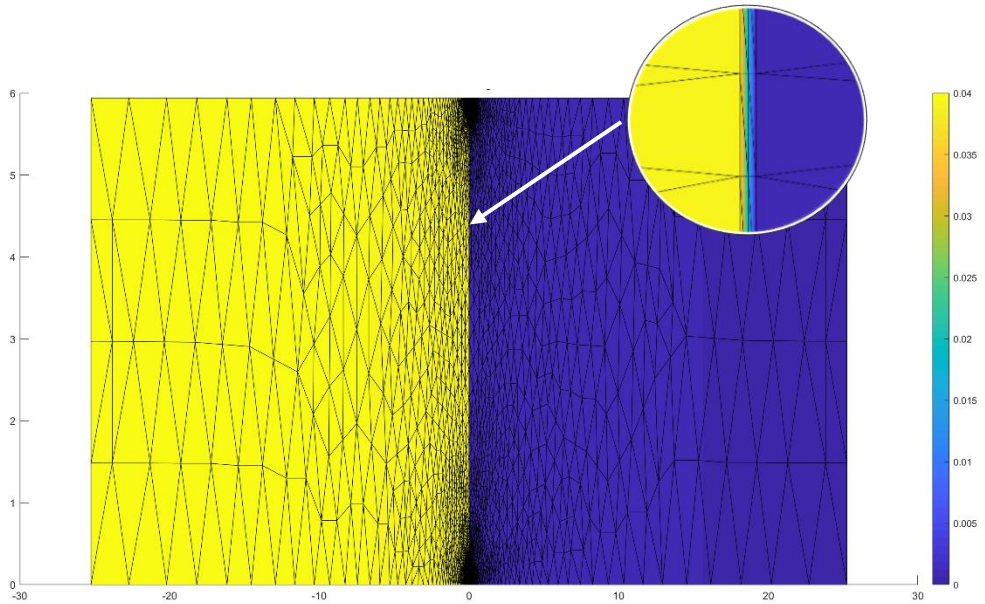

Figure S8. The model outcomes (concentration in nodes) after 5 hours. Related to Figure 5.

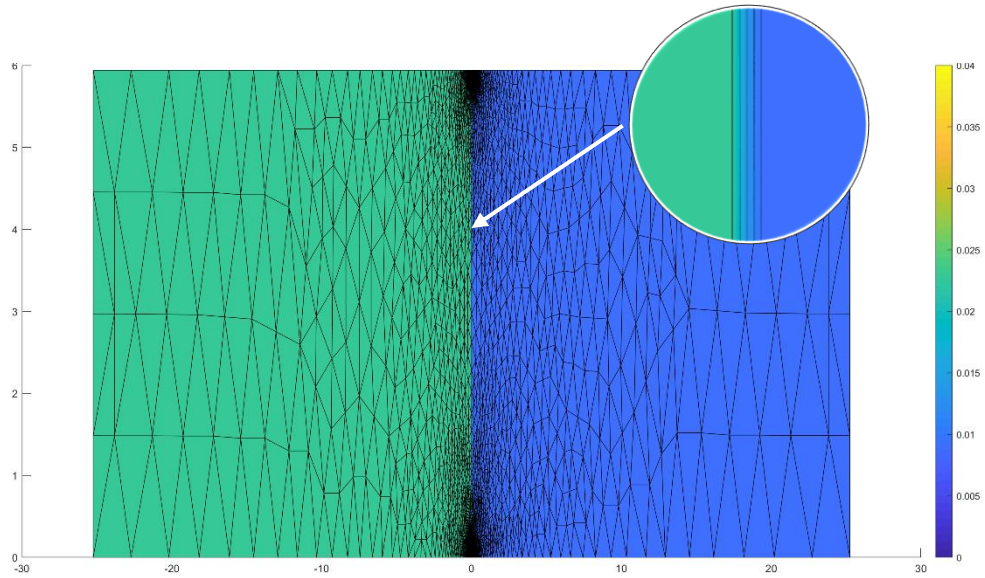

Figure S9. The model outcomes (concentration in nodes) after 115 hours. Related to Figure 5.

Supplemental references:

ALGERS, J., SPERR, P., EGGER, W., KÖGEL, G. & MAURER, F. H. 2003. Median implantation depth and implantation profile of 3–18 keV positrons in amorphous polymers. *Physical Review B,* 67**,** 125404.

BICHSEL, B. 1979. Diffusion phenomena during the decaffeination of coffee beans. *Food Chemistry,* 4**,** 53-62.

EGGER, W., SPERR, P., KÖGEL, G. & DOLLINGER, G. 2007. Pulsed low energy positron system (PLEPS) at the Munich research reactor FRM II. *physica status solidi c,* 4**,** 3969-3972.

ELDRUP, M., LIGHTBODY, D. & SHERWOOD, J. N. 1981. The temperature dependence of positron lifetimes in solid pivalic acid. *Chemical Physics,* 63**,** 51-58.

GSI ENVIRONMENTAL. 2020a. *https://www.gsi-net.com/en/publications/gsi-chemical-database/single/37-atrazine.html* [Online]. [Accessed 23.08. 2020].

GSI ENVIRONMENTAL. 2020b. *https://www.gsi-net.com/en/publications/gsi-chemical-database/single/220-CAS-60515.html* [Online]. [Accessed 23.08. 2020].

GSI ENVIRONMENTAL. 2020c. *https://www.gsi-net.com/en/publications/gsi-chemical-database/single/246-diuron.html* [Online]. [Accessed 23.08. 2020].

GSI ENVIRONMENTAL. 2020d. *https://www.gsi-net.com/en/publications/gsi-chemical-database/single/482-CAS-122349.html* [Online]. [Accessed 23.08. 2020].

HTTPS://CHEMICALIZE.COM. 2019. *Chemicalize was used for name to structure generation/prediction of physicochemical properties of OMPs,17.12. 2019, https://chemicalize.com/ developed by ChemAxon (http://www.chemaxon.com).* [Online]. [Accessed].

HUGENSCHMIDT, C., DOLLINGER, G., EGGER, W., KÖGEL, G., LÖWE, B., MAYER, J., PIKART, P., PIOCHACZ, C., REPPER, R. & SCHRECKENBACH, K. 2008. Surface and bulk investigations at the high intensity positron beam facility NEPOMUC. *Applied surface science,* 255**,** 29-32.

HUGENSCHMIDT, C., PIOCHACZ, C., REINER, M. & SCHRECKENBACH, K. 2012. The NEPOMUC upgrade and advanced positron beam experiments. *New Journal of Physics,* 14**,** 055027.

KIRKEGAARD, P., OLSEN, J. V. & ELDRUP, M. M. 2017. PALSfit3: A software package for analysing positron lifetime spectra.

MA, L., GUTIERREZ, L., VANOPPEN, M., AUBRY, C. & VERLIEFDE, A. 2018. Transport of uncharged organics in ion-exchange membranes: experimental validation of the solution-diffusion model. *Journal of Membrane Science,* 564**,** 773-781.

SPERR, P., EGGER, W., KÖGEL, G., DOLLINGER, G., HUGENSCHMIDT, C., REPPER, R. & PIOCHACZ, C. 2008. Status of the pulsed low energy positron beam system (PLEPS) at the Munich Research Reactor FRM-II. *Applied surface science,* 255**,** 35-38.

TAO, S. 1972. Positronium annihilation in molecular substances. *The Journal of Chemical Physics,* 56**,** 5499-5510.